The Plant Cell, 2026, 38, 1–22
https://doi.org/10.1093/plcell/koag196
Published: 25 June 2026
Large-Scale Biology

The mRNA covalent modification dihydrouridine regulates transcript turnover and photosynthetic capacity during plant abiotic stress

Li'ang Yu [1], Giovanni Melandri [2,3], Anna C. Nelson Dittrich[1], Sebastian Calleja [2], Diep R. Ganguly [4], Kyle Palos [1], Emily K. Brewer [1], Hillary Fischer [5], Bruno Rozzi [2], Aparna Srinivasan [1], Toshihiro Obata [6], Hamada AbdElgawad [7], Gerrit T.S. Beemster [7], Riley Henderson [1], Ciara Garcia [2], Xiaodan Zhang [1], David Stern [1], Andrea Eveland [8], Eric Lyons [2], A. Elizabeth Arnold [2,3], Aleksandra Skirycz [5], Susan J. Schroeder [9,10], Brian D. Gregory [4]*, Duke Pauli [2,3]*, and Andrew D.L. Nelson [1]*

[1]Boyce Thompson Institute, Cornell University, 533 Tower Road, Ithaca, NY 14853, United States
[2]School of Plant Sciences, University of Arizona, 1140 E South Campus Dr., Tucson, AZ 85721, United States
[3]Center for Agroecosystem Research in the Desert (ARID), University of Arizona, 1140 E. South Campus Drive, Tucson, AZ 85721, United States
[4]Department of Biology, University of Pennsylvania, 433 South University Avenue, Philadelphia, PA 19104, United States
[5]Department of Biochemistry and Molecular Biology, Michigan State University, 603 Wilson Rd, East Lansing, MI 48824, United States
[6]Department of Biochemistry and Center for Plant Science Innovation, University of Nebraska-Lincoln, 1901 Vine Street, NE 68588, United States
[7]Integrated Molecular Plant Physiology Research, University of Antwerp, Groenenborgerlaan 171, Antwerp 2020, Belgium
[8]Donald Danforth Plant Science Center, 975 N Warson Rd, St. Louis, MO 63132, United States
[9]Department of Chemistry and Biochemistry, The University of Oklahoma, 101 Stephenson Parkway, Norman, OK 73019, United States
[10]School of Biological Sciences, The University of Oklahoma, 730 & 770 Van Vleet Oval, Norman, OK 73019, United States

*Corresponding authors: Email: an425@cornell.edu or dukepauli@arizona.edu or bdgregor@sas.upenn.edu
The authors responsible for distribution of materials integral to the findings presented in this article in accordance with the policy described in the Instructions for Authors (https://academic.oup.com/plcell/pages/General-Instructions) are: Andrew D. L. Nelson, Duke Pauli, and Brian D. Gregory.

Abstract

RNA covalent modifications (RCMs) influence RNA stability and translation efficiency, and they thus play critical roles in eukaryotic growth and development. However, their role in regulating plant performance under abiotic stress remains largely unexplored. Here, we integrated multi-omics data in 6 *Sorghum bicolor* accessions under water-limiting conditions in the field to explore the relationship between RCMs and drought response. Within a stress- and photosynthesis-associated gene co-expression module, we identified *SbDUS2*, a member of a family of enzymes conserved across eukaryotes, that catalyzes the reduction of uracil to dihydrouridine (DHU) on RNA molecules. DHU-modified transcripts in this module were enriched for photosynthetic functions and showed strong correlation with photosynthetic traits. To elucidate the function of this RCM, we characterized loss-of-function *dus2* mutants in *Arabidopsis thaliana*. Under control conditions, these DHU-deficient mutants exhibited impaired germination and delayed development. Furthermore, under water-limiting or heat conditions, these mutants showed significantly reduced net CO_2 assimilation and survival. Using multiple transcriptome-wide RNA stability assays, we demonstrated that transcripts associated with lower DHU levels in a *dus2* background generally exhibited increased stability compared to Col-0 controls. Particularly, lack of DUS2 led to the hyperstability of photosynthesis-related transcripts, impeding their turnover and likely preventing proper photosynthetic acclimation during stress. We propose a model where DHU acts as a critical post-transcriptional regulator marking mRNAs for rapid turnover under stress, highlighting an overlooked regulatory layer contributing to plant resilience.

Received: November 24, 2025. **Accepted:** May 16, 2026

Introduction

Agricultural production faces intensifying challenges as drought and heat stressors increase in frequency and severity across major cropping regions (Alizadeh et al. 2020). These abiotic stressors trigger a range of adverse phenotypic and physiological responses, including heightened susceptibility to biotic stresses, altered development, and reduced yield. Consequently, enhancing plant productivity and resilience under such conditions has become a primary goal in improving stress tolerance. A widely adopted strategy to achieve this goal involves the exploration and utilization of genetic variation (Glaszmann et al. 2010; Khoury et al. 2022). While large population-level studies within many crop species have identified strong abiotic stress tolerance phenotypes and associated loci useful for breeding and selection (Gilliham et al. 2017), the crosstalk between many upstream regulatory genes and downstream trait-associated genes remains unclear and largely unexplored. In addition to feedback at the DNA, RNA, and protein level, there are additional levels of regulatory control that make identifying beneficial alleles for crop improvement more challenging.

RNAs endure numerous co- and post-transcriptional events that influence their function, one of which is the covalent modification, or isomerization, of RNA bases. RNA covalent modifications (RCMs) are an emerging and underexplored layer of regulation in eukaryotes (Harcourt et al. 2017; Roundtree et al. 2017). RCMs are widespread and chemically diverse, decorating all classes of RNA, non-coding and coding alike (Finet et al. 2022b). As a natural result of their higher abundance, most RCMs were first characterized on housekeeping RNAs such as tRNAs and rRNAs (Yu et al. 2011; Toubdji et al. 2024). One such RCM is dihydrouridine (DHU), which is formed by the reduction of the double bond in uridine by a highly conserved class of dihydrouridine synthase (DUS) enzymes (Yu et al. 2011). DHU is known to disrupt base stacking and increase RNA flexibility, particularly in tRNAs, where it is critical for the formation and function of the D-loop (Toubdji et al. 2024), a role that is conserved across all living organisms (Chen et al. 2010; Lombard et al. 2022; Ju et al. 2025). In non-plant systems, DHU has recently been found in yeast mRNAs, and at low stoichiometry in human mRNAs, predominantly in transcripts associated with core cellular mechanisms (Kato et al. 2005; Rider et al. 2009; Ju et al. 2025). Disruption or depletion of DHU from these transcripts results in growth defects in yeast and, in humans, enhanced tumorigenesis (Kato et al. 2005; Rider et al. 2009). Despite the growing evidence that DHU plays an important role in mRNAs, how DHU regulates mRNA function, and the extent to which this RCM is present in plant mRNAs, is unclear.

Much of what we know about mRNA-associated RCMs comes from studies on N6-methyladenosine (m^6A), which has been shown to influence plant development and stress responses by modulating mRNA fate (Zhou et al. 2022; Liu et al. 2025; Shao et al. 2025). RCMs are known to regulate RNA stability, structure, translation, and localization within, and potentially between, cells (Anderson et al. 2018; Arribas-Hernández et al. 2018; Luo et al. 2020; Cheng et al. 2021; Prall et al. 2023). Despite this growing appreciation of the roles that RCMs can perform, many evolutionarily conserved RCMs, such as DHU, pseudouridine (Ψ), N^1-methyladenosine (m^1A), and 5-methylcytidine (m^5C), remain largely unknown in plants (Tang et al. 2020; Yang et al. 2020; Li et al. 2025). This knowledge gap stems in part from technical barriers. Several RCMs can be detected with antibody-based methods (Dominissini et al. 2012; Meyer et al. 2012; Edelheit et al. 2013; Li et al. 2016), and more recently at the transcript level using Oxford Nanopore direct RNA-seq (DRS) along with trained algorithms to detect specific modified ribonucleotides (Garalde et al. 2018; LaPierre et al. 2019; Liu et al. 2019; Wu et al. 2024; Cruciani et al. 2025). For modifications that impact the base-pairing edge, bioinformatic approaches that interpret the pattern of resulting reverse transcription (RT)-induced errors at modified sites have been deployed with great success (Ryvkin et al. 2013; Tan et al. 2021). Although the resolution is somewhat limited to highly abundant transcripts due to the reliance on sufficient read depth for accurate detection and classification (Helm and Motorin 2017), these approaches have nevertheless been helpful in extending insights into the roles of less-studied RCMs (Sharma et al. 2023).

Sorghum [*Sorghum bicolor* (L.) Moench] is a heat- and drought-tolerant crop widely cultivated for grain, forage, and cellulosic biomass production (Lobell et al. 2008; Abreha et al. 2021). Due to its phylogenetic placement within the *Poaceae*, findings from sorghum often transfer to other critical agronomic crops such as *Zea mays*. A well-annotated genome (McCormick et al. 2018), along with the physiological and morphological variation found within multiple diversity panels (Morris et al. 2013; Boatwright et al. 2022; Wu et al. 2022), make sorghum ideal for supporting comparative, systems-level analyses on field-grown plants. Indeed, several studies have used these resources to highlight transcriptional responses to heat and drought stress in sorghum, uncovering genetic factors that might contribute to improved stress resilience in sorghum and other important grasses (Boyles et al. 2019; Varoquaux et al. 2019). Thus, these resources and characteristics make sorghum ideally suited for uncovering RNA-based regulatory mechanisms contributing to plant resilience.

Here we leveraged a systems biology approach to study how 6 phylogenetically distinct sorghum accessions with different levels of drought tolerance respond to water-limiting conditions over time. Our integrative approach using global-wide datasets identified the transcripts with DHU modification and its corresponding enzyme for DHU synthesis in sorghum, SbDUS2, as strongly associated with plant photosynthetic performance in the field. Interestingly, SbDUS2 is orthologous to human and fission yeast DUS2, which were both previously found to be responsible for mRNA DHU deposition. Given the deeply conserved nature of the DUS enzymes, we turned to *Arabidopsis thaliana*, where genetic *loss-of-function* mutants for the orthologous DUS2 were available, to investigate the functional role of DHU in *Arabidopsis*. Under control conditions, *Atdus2* mutants displayed reduced germination and delayed growth relative to *AtDus2* controls. A set of complementary approaches was used to confirm that Arabidopsis *dus2* mutants displayed reduced DHU levels, particularly on mRNAs associated with photosynthesis and metabolism. After confirming that *Atdus2* mutants displayed reduced DHU levels on mRNAs, we used this background to better understand the role of DHU in plant stress responses. Interestingly, *Atdus2* mutants exhibited a similar physiological response to drought and heat, showing reduced CO_2 assimilation and lower survival. In Col-0 controls under heat, but not in the *Atdus2* background, photosynthesis-related transcripts were found to be differentially DHU-modified, a phenomenon that coincided with decreased abundance for the associated transcripts. Using a transcriptional arrest time course–derived RNA decay assay at a global level, we demonstrated that DHU predominantly destabilizes mRNAs under control and abiotic stress conditions in Arabidopsis, and we propose a model whereby DHU is critical for mRNA turnover, particularly under stress scenarios, highlighting the

significance of this overlooked regulatory mechanism with real-world agronomic relevance.

Results

Development of a diverse set of sorghum accessions with variation in their molecular and physiological responses to abiotic stress

Phenotypic diversity under drought conditions is ultimately traced to variation in genomic sequence and rewiring of gene expression. Therefore, to capture the genetic and phenotypic diversity present within sorghum, we initially generated a phylogeny from re-sequencing data for 356 out of 400 accessions with demographic information found within the sorghum association panel (SAP, Fig. 1a, File S1) This panel has been widely used in the community for drought and heat studies (Boatwright et al. 2022), providing a well-characterized resource for evaluating stress responses (da Bernardino et al. 2024; Singh et al. 2025). Cross-referencing this phylogeny with the SAP field trial (in Arizona in 2019) under standard conditions, we selected 6 accessions to comprise a small but diverse panel based on seed viability, genetic distinctiveness, and phenotypic variation (shoot and root biomass, plant height, and yield). Among the selected lines, 4 accessions (A, B, E, and F) are African accessions, and the other 2 accessions (C and D) are US breeding accessions (Fig. 1a). Variant calling and annotation of variants were performed to examine the genomic variation between these accessions. In total, 8,725,449 variants were identified among the 6 accessions relative to the published reference genome, with more than 50% of variants located in intergenic regions, followed by upstream and downstream gene regulatory regions (21.0% and 19.5%, respectively), intronic regions (5.61%), and splicing regions (0.23%; Figure S1, left panel). Approximately 10% to 20% of the genomic variation in the panel was comprised of unique single nucleotide polymorphisms (SNPs) and insertion/deletions (INDELs) specific to each genotype (Figure S1, right panel). In summary, these data suggest that we were successful in selecting 6 distinct accessions, representative of the genetic diversity within the species, and likely the wide range of environments in which sorghum can grow.

To assess the performance of this panel, we grew the 6 accessions in replicated plots as part of a large field trial conducted in the summer of 2020 at the Maricopa Agricultural Center, a setting characterized by consistently elevated temperatures and extreme vapor pressure deficits (VPDs). All plants were well-watered (WW) until the beginning of the reproductive stage (appearance of the flag leaf; 47 days after planting; Fig. 1b), after which irrigation was reduced for a subset of plots to mimic drought treatment. Phenotypic measurements and molecular sampling (for transcriptomic, metabolomic, and biochemical traits) occurred during the first, third, fifth, and seventh week after the beginning of the drought treatment (Fig. 1b), with destructive measurements (eg biomass and root microbiome composition) occurring at the end of the season. Treatment effects were readily apparent at the end of the season (Fig. 1c), with the M1 ("A") accession showing the most pronounced leaf necrosis. Leaf-level physiological traits, such as water use efficiency (WUE) and CO_2 net assimilation (internal) exhibited similar results, with the "A" accession displaying hallmarks of water stress, particularly at the later time points (week 5 and week 7, Fig. 1d), whereas other accessions, such as "B" and "C," showed a more robust response. Thus, in addition to genotypic diversity, these data suggest that these 6 accessions displayed phenotypic diversity to drought stress and may provide information on the molecular mechanisms by which sorghum responds to water-limiting conditions.

Sorghum accessions display variable molecular responses to stress

To characterize the molecular responses to water-limiting conditions in our panel, we next assessed the change in transcript abundance over the 2 months of the treatment (weeks 1, 3, 5, and 7) using RNA-seq. Initial quality control revealed high correlation between replicates (Pearson correlation; $r > 0.95$, Table S1). To unpack the transcriptomic responses to treatment in the 6 accessions, we examined the top 10% of most variable transcripts based on the standard deviation of the global transcript abundance for principal component analysis (PCA). This approach uncovered strong genotypic and treatment effects represented by both principal component 1 (PC1) and PC2, with accession "C" exhibiting the least separation due to stress or time, and accession "A" exhibiting the most (PC1 = 19.35%, PC2 = 14.88%, Fig. 1e).

To gather additional clues as to how these accessions responded to drought treatment at the molecular level, we next examined the stress-induced changes in metabolites and oxidative stress markers in sorghum leaves (Das and Roychoudhury 2014; Obata et al. 2015). Metabolites and oxidative stress markers were measured on leaf samples collected simultaneously with those used for RNA-seq analyses, with gas chromatography–mass spectrometry (GC-MS)-based quantification and annotation of primary metabolites and spectrophotometric-based quantification of oxidative stress markers. A PCA of global changes in the leaf primary metabolome ($N = 46$) across our panel revealed that, as for the transcriptome, genotype explained much of the variation between samples (Fig. 1f, left panel; PC1: 33.25%). Interestingly, samples associated with accession "A," weeks 3, 5, and 7 (both conditions), separated from all other samples, and this separation was largely driven by levels of the 3 main soluble sugars (sucrose, glucose, and fructose) and chlorogenic acid (Fig. 1f, right panel). Overall, we identified strong genotypic effects for both visible and molecular phenotypes. As expected for this species, most accessions displayed resilience under stressed conditions, whereas accession "A" performed poorly in under stress conditions. Thus, this panel presents a suitable comparative framework to examine transcriptional and post-transcriptional regulators of drought and heat stress responses in sorghum under field conditions.

Integrated network analysis uncovers a link between DHU and photosynthesis traits

With each of these molecular and physiological traits examined, we next took a comparative systems-level approach to connect these traits to their molecular pathways and putative regulators. To do so, we constructed a co-expression network starting with the top 10% of most variable transcripts, as measured by median absolute deviation (MAD) score. We then recursively increased the number of included transcripts until we achieved an optimized network with the fewest number of unassigned transcripts and the highest scale-free topology model (Table S2). The resulting network contained 22,314 transcripts classified into 29 modules with a low proportion of unclassified transcripts ($N = 2{,}982$) and high scale-free model correlation ($r = 0.91$, slope = −1.93, Table S2). Using this framework, we incorporated phenotypic data into modules using trait-module correlation. Briefly, the

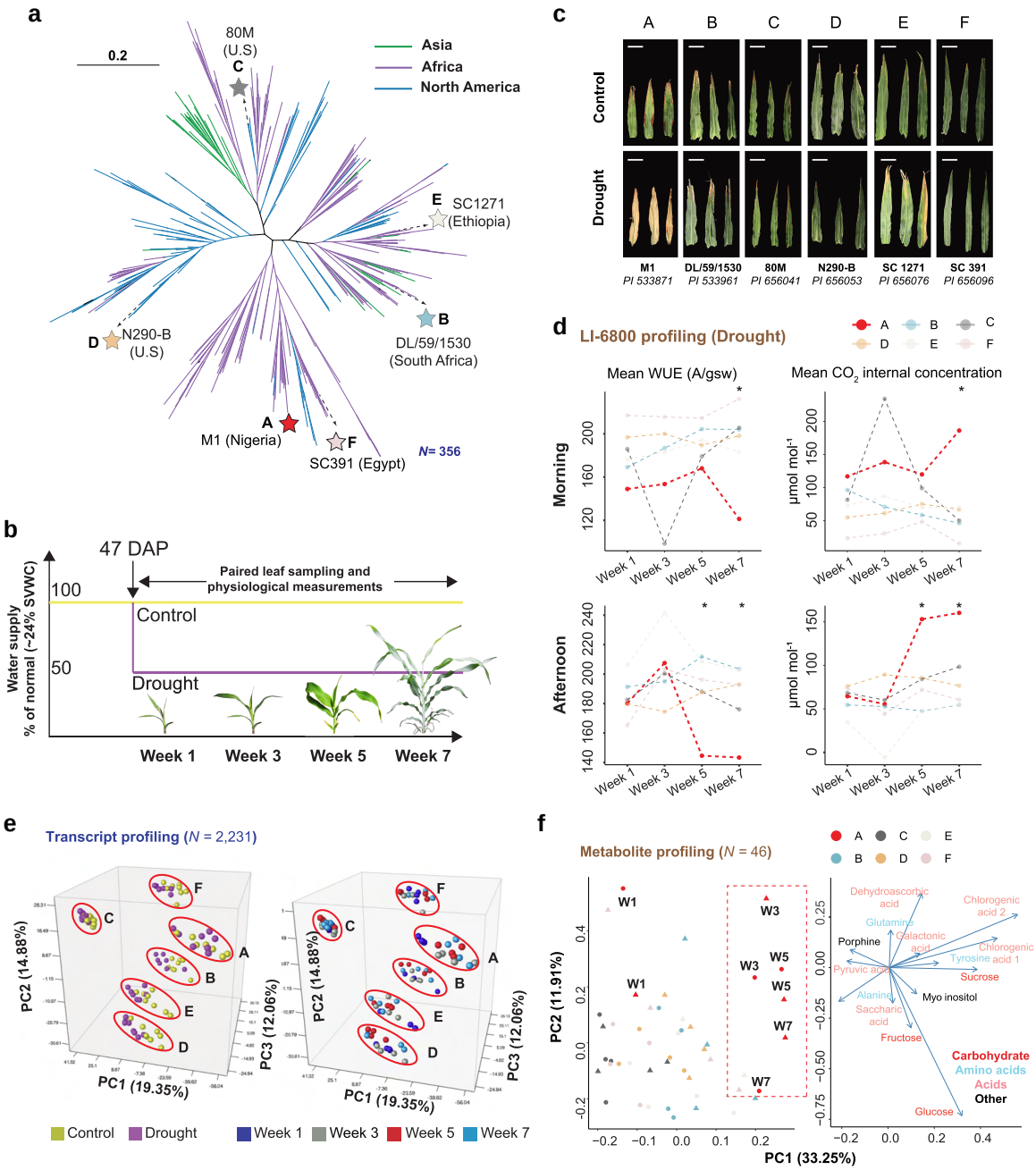

Figure 1 Drought tolerance diversity of selected sorghum genotypes. (a) Reconstruction of an unrooted phylogeny of the Sorghum Association Panel (SAP). The 6 sorghum accessions used in this study are marked along with the geographical locations colored to represent African, Asian, and North American regions. The placement of the 6 accessions used in this study is denoted with different colored stars that match the color scheme throughout this work. (b) Six sorghum accessions were grown at the Arizona in the field with treatment (reduced water supply) imposed 47 days after planting (DAP). Paired molecular sampling (RNA-Seq, metabolites, and oxidative stress chemicals), were collected alongside physiological measurements (eg LI-6800 photosynthesis-related traits). (c) Representative leaf tissue collected at the terminal stage of sampling in the field is shown with images digitally extracted for comparison, alongside scale bars (5 cm, white lines) displayed for each image. (d) Line graphs denote the mean WUEi and internal CO_2 concentration values measured during the morning (top) and afternoon (bottom) at each time point for drought-treated plants ($N = 5$ per accession). Asterisks indicate significant differences of parameters derived from the comparison of each accession relative to "A" using pairwise Student *t* test ($P < 0.05$ marked with an asterisk). (e) Two principal component analyses (PCAs), based on the top 10% most abundant transcripts, highlight the separation caused by genotypic and treatment effects (left) and genotypic and temporal effects (right). (f) The left PCA displays separation based on treatment (triangle = drought; circle = control) and genotype (colors similar to those in panel c). The right PCA loading plot highlights major contributors to the left PCA, with the length of the line denoting the contribution of a particular molecule to the PCA.

first principal component value (eigenvalue) per module was calculated using their transcript abundance in PCA. Leaf-level physiological measurements (LI-6800), metabolite abundances, and oxidative stress marker abundances were then correlated with the eigenvalues of each module (Table S3), leading to 19 modules with significant trait-module correlations ($P < 0.05$, Fig. 2a, left panel). Several modules

(eg "blue," "greenyellow," "pink," and "purple") were strongly correlated with multiple traits. For instance, "blue," "purple," and "pink" modules are closely related to most photosynthesis traits (> 90% LI-6800 entries), whereas "purple" and "greenyellow" modules are highly correlated with many metabolic traits and oxidative stress chemical abundances (Fig. 2a).

To gain insights into the biological processes associated with modules, module-wise Gene Ontology (GO) and Kyoto Encyclopedia of Genes and Genomes (KEGG) enrichment analyses were performed (modules with *FDR* < 0.05 are displayed, Fig. 2a, top panel). This approach revealed modules with biological processes of interest, such as stress response ("blue," "red," and "pink"), RNA processing and modification pathways ("blue," "greenyellow," "purple," "midnightblue," and "lightyellow"), and photosynthesis terms ("blue," Fig. 2a and Table S4). Specifically, in addition to the observed module-trait correlation, the "blue" module was strongly enriched for transcripts associated with photosynthesis traits (eg net CO_2 assimilation: $r = 0.72$) based on both GO and KEGG terms (fold change > 5, *FDR* < 0.05, Table S4). Interestingly, an examination of eigengene values within this module revealed a strong genotypic effect, where transcripts derived from the "A" accession cluster separately from the other accessions (Fig. 2b), and therefore may explain the physiological distinctiveness of this accession. Given the strong trait module correlations and the overrepresentation of stress- and photosynthesis-associated genes, the "blue" module thus represents a strong link between phenotypic and molecular responses to stress treatment.

To identify genes closely associated with the overall expression pattern (eigengene value) of the blue module, we calculated module membership (kME) values for each transcript as the correlation between its change in abundance and the module eigengene. Among the top 10% of genes ranked by kME, 2 were annotated as putative dihydrouridine synthases (DUS; Sobic.006G158100 and Sobic.006G038500, Table S5), enzymes that convert uridine to dihydrouridine (DHU). A phylogenetic analysis using a maximum likelihood tree derived from an amino acid sequence alignment of human, fission yeast, budding yeast, and multiple plant DUS proteins (Files S2 and S3) suggests that Sobic.006G158100 is more similar to eukaryotic DUS2 (Figure S2; SbDUS2), whereas Sobic.006G038500 fell into the DUS3 clade (Figure S2; SbDUS3). A third sorghum DUS, Sobic.010G262000, fell into the DUS1 clade but was not found to be associated with plant performance traits within the "blue" module (SbDUS1). The strong association between these 2 genes and the blue module implies that their transcriptional regulation, and potentially their function, is associated with plant performance under stress.

Given the inclusion of DHU synthase in the stress and photosynthesis-related "blue" module, we examined the RNA-seq data for hallmarks of RCMs that impact the Watson-Crick-Franklin base-pairing edge. DHU belongs to a subset of RCMs that interfere with RNA-seq library preparation (specifically the reverse transcription step), leaving patterns of mis-incorporated nucleotides that can be assigned to specific modification classes bioinformatically (Vandivier et al. 2015; Helm and Motorin 2017; Tan et al. 2021). We thus processed our RNA-seq data through 2 independent RCM predictors (HAMR and Modtect) and took the intersection of called sites (Table S6), resulting in 20,096 high-confidence RCMs associated with 3,715 transcripts among the 6 main classes of HAMR/Modtect identifiable RCMs (Table S7). Of these, a total of 3,008 DHU sites on 1,370 transcripts were detected, with 326 transcripts associated with predicted DHU modification residing within the "blue" module (Table S8). The 3,008 DHU-associated transcripts were enriched in multiple metabolism-related terms, consistent with patterns reported for other RCMs (Figure S3A). Although overall DHU levels did not differ significantly among the 6 accessions under either condition (Figure S3B), the proportion of accession-specific DHU transcripts varied, with accession "A" showing the highest number under both conditions (Figure S3C).

To test whether DHU is preferentially associated with photosynthesis- and stress-related transcripts in the "blue" module, we compared GO enrichment between DHU-modified and non-DHU-modified transcripts. Since DHU detection is abundance-dependent and photosynthesis transcripts are often highly expressed, we generated equal-size TPM-matched non-DHU control sets from within and outside the "blue" module for GO enrichment analysis (bootstrap = 5, Figure S4A, Table S9). This approach uncovered an elevated enrichment level of "photosynthesis" and "abiotic stress" terms in the DHU-modified sets compared with the other 2 "non-DHU-modified" sets (Fig. 2c). These results suggest that even in the "blue" photosynthesis- and stress-associated module, there is a further enrichment in photosynthesis-related terms for DHU-modified transcripts that cannot be explained by transcript abundance alone. Lastly, to determine if there was a relationship between DHU abundance and field-derived traits, a pairwise Pearson correlation was performed between transcript abundance and photosynthetic trait measurements (A, Ci, and gsw, respectively) for all DHU-modified and a similar number of randomly selected non-DHU-modified transcripts (Fig. 2d). This analysis revealed a strong correlation between transcripts associated with DHU modification and photosynthetic traits, suggesting a close relationship between DHU modification status, transcript abundance, and photosynthetic processes in sorghum.

We next assessed whether the transcriptomic accession-associated variation was also observed in the DHU deposition on these 326 modified transcripts. A PCA revealed that the DHU status for these transcripts in the "A" accession was markedly different at most time points and conditions relative to the other accessions (PC1 was primarily explained by DHU variation in the "A" accession; Fig. 2e). We explored this accession-driven variation further by determining if the pattern of DHU deposition on these transcripts was different in the "A" accession relative to the others. Based on a metaplot profiling of DHU deposition on the 326 DHU-modified transcripts, we observed variation at both the 5′ and 3′ ends, with the most dramatic variation near the 3′ end of the coding sequence (CDS) in the "A" accession relative to the others (Fig. 2f). In sum, these data highlight the association between DHU status and photosynthesis, suggesting that variation in this molecular phenomenon between accessions be linked to plant performance.

SbDUS2 is associated with DHU deposition on photosynthesis-related transcripts in sorghum under abiotic stress

To determine if *SbDUS2* or *SbDUS3* were more likely to be responsible for DHU deposition on photosynthesis-associated transcripts, we next tested the reproducibility of the transcriptomic interactions visible within the "blue" module. To do so, we first developed a child network of all transcripts in the "blue" module that shared high-confidence edges with *SbDUS2* and *SbDUS3* and were DHU-modified ($N = 29$, Figure S5A and Table S5) and examined the relationship of these transcripts with both *SbDUS2* and *SbDUS3* transcripts and DHU

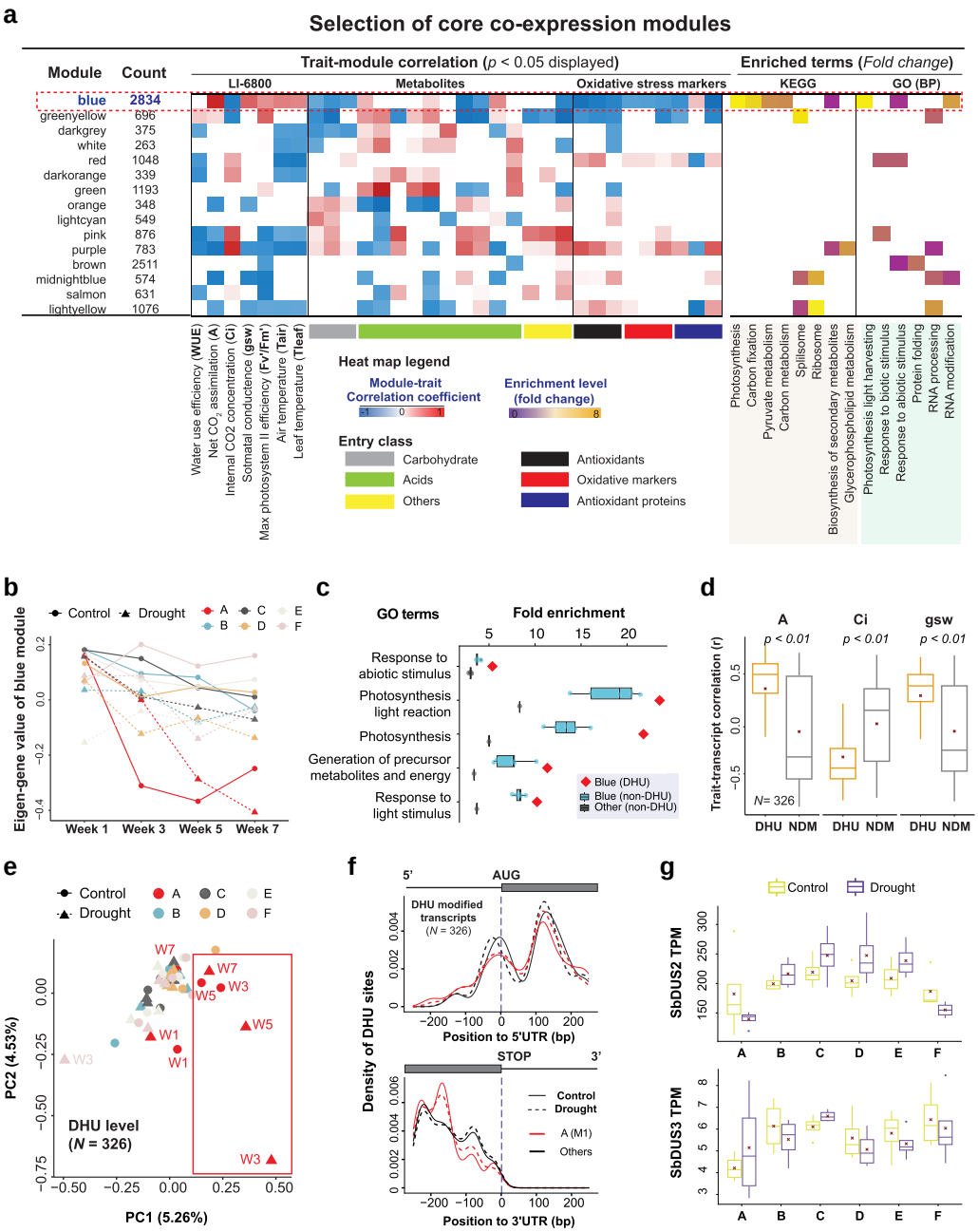

Figure 2 Selection of co-expression modules contributing to sorghum drought tolerance. (a) The number of transcripts per module, correlation between traits and the module, levels of KEGG and GO enrichment levels, and the known proteins related to RCM recognition, deposition, and removal located in each co-expression module. Scales for module-trait correlation values (blue to red scale: −1 to 1), as well as GO-enrichment levels (fold changes) are shown to the bottom left. Only those module-trait correlations and enrichment levels with a $P < 0.05$ are shown. (b) The eigenvalue of the photosynthetic module, divided by accession, treatment, and time, was plotted. (c) Boxplots denote the fold GO term enrichment level of 326 DHU-modified transcripts in the "blue" module (red diamonds) and TPM-matched non-DHU transcripts within and outside the "blue" module (5 bootstraps for TPM each TPM-matched set). (d) Box plots denote the correlation coefficient (r) between transcript abundance and each photosynthetic trait (A, Ci, and gsw) between DHU-modified group and the nonmodified group and compared using Student t test. (e) Principal component analysis (PCA) of DHU-modified transcripts from the "blue" module ($N = 326$ transcripts). (f) Metaplot shows density of DHU sites across upstream (downstream) 250 bp genomic region near start (stop) codon over 325 transcripts in accession "A" and other 5 accessions under control and drought conditions. (g) TPM of *SbDUS2* and *SbDUS3* across the 2 conditions and 6 accessions.

abundance. Interestingly, we observed a negative correlation between DHU status and the abundance of these 29 interacting transcripts in our field data (Figure S5B). We then examined the abundance of each of these transcripts in a publicly available sorghum tissue atlas dataset (McCormick et al. 2018, accession: BTx623), as well as a time-series drought dataset between a sensitive and tolerant accession (Varoquaux et al. 2019). Not only were these 29 DHU-modified transcripts most highly abundant at similar developmental stages in the sorghum tissue atlas as in our dataset, but we also observed a strong negative correlation between DHU levels and

11 out of the 29 focal transcripts across this tissue atlas using HAMR/Modtect ($P < 0.05$; Figure S5C). Notably, *SbDUS2* and *SbDUS3* were also predominantly expressed in leaf tissues, and largely during late vegetative and flowering developmental stages, similar to our observations in our 6 accessions (Figure S5D). We then asked which SbDUS most likely influences DHU deposition on mRNAs within the "blue" module by assessing the correlation between the score of the first principal component (PC1) of 326 transcripts-derived DHU PCA (Fig. 2e) and the transcript abundance of *SbDUS2* and *SbDUS3* (Figure S3E). This analysis revealed a stronger correlation between *SbDUS2* and PC1 scores ($r = -0.63$, $P = 1.4e\text{-}06$) than for *SbDUS3* ($r = -0.39$, $P = 0.0064$), implying that SbDUS2 might be more tightly associated with DHU status. Additionally, *SbDUS2* exhibited significantly higher transcript abundance (TPM) in both datasets ($P < 0.0001$, Figure S5D, and Fig. 2g). Not only was *SbDUS2* on average ~40× more abundant than *SbDUS3* across the 6 accessions and in the sorghum tissue atlas data, Sb*DUS2* also displayed an overall decreased transcript abundance under water-limiting conditions in the "A" and "F" accessions and an increase in all other accessions (Fig. 2g), whereas *SbDUS3* displayed no significant treatment effect. We also assessed *SbDUS1*, which was more highly abundant than *SbDUS3*, but did not associate with transcripts in the "blue" module or performance-related traits and displayed minimal transcript-level differences in response to treatment across file data and the public drought dataset (Figure S5F and S5G). Thus, based on its expression pattern across multiple datasets and strong correlation between DHU and *SbDUS2* transcript abundance, we hypothesize that SbDUS2 is largely responsible for changes in DHU abundance across genotypes and treatments, although we cannot rule out the contribution of the other DUS enzymes to DHU deposition on different RNA classes, or under other conditions.

DUS2 mutants display DHU level reduction associated with growth and developmental delays in Arabidopsis

Convinced that DHU was somehow linked to photosynthetic traits in sorghum, and that SbDUS2 was the likely enzyme responsible for DHU deposition on photosynthesis-associated transcripts, we next turned to the genetic model *Arabidopsis thaliana* to gain a better understanding of how DHU might impact plant performance. Based on our phylogenetic assessment of the DUS1/2/3 protein family across eukaryotes, we identified the Arabidopsis *Dus2* ortholog, which encodes a protein that is 79.81% identical to SbDUS2 at the amino acid level (Figure S2 and Fig. 3a). We obtained 2 T-DNA insertion lines that disrupted the third and fourth exons, respectively, within the coding region of *AtDus2* (AT3G49640, Fig. 3a, CS857388 and SALK_079129C, https://abrc.osu.edu/). We confirmed that these insertions disrupted *AtDUS2* transcription using both Illumina and Oxford direct RNA-seq (ONT-DRS; Figure S6A).

To determine the impact of AtDUS2 on different RNA classes, we purified mRNA from total RNA in Col-0 and *dus2*, supported by successful depletion of rRNA/tRNA in our mRNA fraction as determined by fragment analyzer profiling (Figure S7), and then performed liquid chromatography with tandem mass spectrometry (LC-MS/MS) to detect DHU abundance. We observed DHU in the mRNA-depleted, total RNA samples (rRNA + tRNA), likely driven by tRNAs (Fig. 3b). In addition, we observed DHU in mRNAs, although at levels approximately 100× lower than in the tRNA fraction, consistent with prior studies in yeast and human mRNAs (Fig. 3b; Finet et al. 2022a; Ju et al. 2025). While we observed a significant decrease in the amount of DHU found in the mRNA-depleted samples (ie tRNAs) in the *dus2* −/− background, we only observed a modest reduction in mRNAs (Fig. 3b, left; Table S10; $P = 0.022$, and $P = 0.71$, respectively). Using our ModTect/HAMR approach, we did, however, observe a slight but significant decrease in the ratio of modified reads reported across the transcriptome in the *dus2* background compared to the wild type (Col-0; Fig. 3c, left). Of note, ModTect/HAMR report a mean transcript-level ratio of modified reads rather than the absolute abundance of that modification as is measured by LC-MS/MS. Thus, we also incorporated a transcript level analysis, using ONT-DRS. Although a DHU-aware base-calling algorithm is not currently available for ONT-DRS, we used ONT-DRS to detect differentially "modified" U sites between Col-0 and the *dus2* background that were not associated with the 2 currently detectable Uracil modifications, Ψ or 2′-O-Me-U (Fig. 3c, right). After excluding these modifications, we observed a slight reduction in modified U sites in *dus2* relative to the Col-0 background and also observed a shift in the transcripts that were modified, consistent with the LC-MS/MS quantification and suggesting that these modified sites are AtDUS2 dependent. Based on HAMR/Modtect-derived data in both Arabidopsis (Col-0) and sorghum samples, we observed DHU being deposited in a similar U-tract sequence context within mRNAs as was observed in yeast (Figure S8A), with a preference for the CDS over UTRs (Figure S8B, Finet et al. 2022b). These data suggest that DHU is found within Arabidopsis mRNAs and that at least a subset of them are dependent on AtDUS2.

In addition to diminished DHU levels, Arabidopsis *dus2* mutants displayed reduced germination (Fig. 3d left; $P < 0.05$, $N > 50$) and slower growth rates, as well as shorter stature and increased time to flower in both *Atdus2* mutant lines relative to wild-type controls (Col-0, Fig. 3d right), although the *Atdus2* mutants eventually reach normal height relative to Col-0 (Figure S6B). To further strengthen the causality of *Atdus2*-dependent effects on plant growth and development, we introduced AtDUS2 with a C-terminal 3xFLAG epitope driven by the CaMV 35S promoter into the *dus2* (−/−) mutant background (CS857388) and verified expression of the protein via Western blotting (Figure S6C). Two independent complementation lines were able to successfully rescue the defects in delayed growth and flowering observed in the mutant plants (Fig. 3e). Ultimately, these transgenic experiments confirm that loss of *AtDUS2* leads to abnormal growth and development under control conditions.

Given the importance of DHU for function of other classes of RNAs, we next assessed whether the *Atdus2* mutant background exhibited an mRNA- and protein-level response that might explain the observed delayed growth phenotype. To explore transcriptomic and proteomic responses, we compared profiles from mature rosette leaves of *Atdus2* mutants vs Col-0 controls. Illumina RNA-seq was used to determine which transcripts were differentially abundant and untargeted LC-MS/MS was used to determine if protein abundance was impaired by loss of *AtDus2*. Loss of *AtDus2* led to 807 and 1,096 transcripts with increased and decreased abundance, respectively ($FDR < 0.05$, $|\log_2\text{-FC}| > 1$; Figure S9A, Table S11). At the protein level, 2,901 proteins with reproducible detection across replicates ($N = 3$ per genotype) were examined for changes in abundance between *Atdus2* and Col-0. We found 128 and 147 proteins with increased or decreased abundance ($padj < 0.05$; Figure S9b), respectively, in the mutant, with a strong positive correlation in the change between genotypes between transcript and protein abundance observed for those where matching data were available ($N = 275$, $r = 0.43$ and $P = 1.7e\text{-}13$,

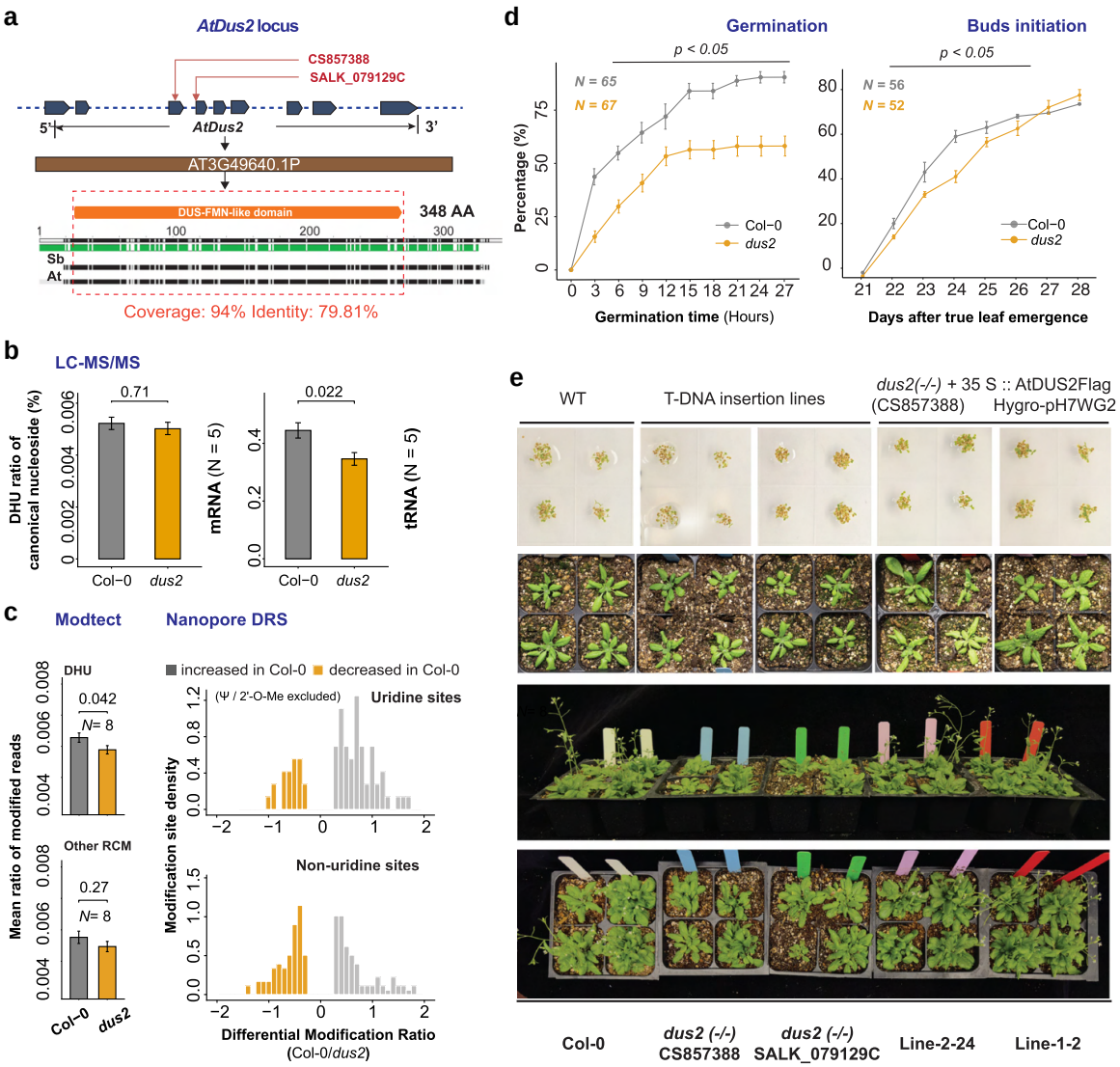

Figure 3 Characterization of the *dus2* mutant in Arabidopsis. (a) Schematic of the *AtDUS2* locus (top) with the T-DNA insertion sites in the third and fourth exon denoted. A protein alignment of the Arabidopsis and sorghum DUS2 proteins is depicted below, with the DUS-FMN-like domain outlined in orange. Alignment coverage and amino acid identity is shown below. (b) Comparison of 5,6-dihydrouridine between Col-0 and *dus2* background using LC-MS/MS analysis of hydrolyzed mRNA (left) and tRNA (right, mRNA-depleted fraction) with the normalized ratio of DHU over 4 canonical nucleosides displayed (%). Significance for (b–c) determined by Student *t* test. (c) Left: DHU mRNA modification frequency, derived from Illumina RNA-Sequencing and determined with ModTect/HAMR, is shown for Col-0 and Atdus2 mutant backgrounds. Right: Density plot of significantly modified sites (q-value < 0.05) between Col-0 and *dus2* of uridine-associated/non-uridine-associated sites using Nanopore DRS. (d) Left**:** Profiling of seeds grown on MS plates, with each datapoint representing 3 plates. Germination rate was calculated as the full emergence of cotyledons with images after 2-day germination; Right**:** Bud initiation rate of Col-0 and Atdus2 plants: Percent of plants with flower buds visible plotted over time are recorded. (e) Phenotypic characterization of Col-0 (WT), 2 *dus2* T-DNA insertion lines (CS857388 and SALK_079129C), and 2 independent DUS2–3×FLAG-pH7WG2 rescue lines at different developmental stages.

Figure S9C). We then integrated the status of RNA, DHU, and protein abundance in the 2 genetic backgrounds, focusing on a set of 38 DHU-modified transcripts that displayed differential abundance at all 3 levels between Col-0 and *Atdus2* backgrounds (Table S12). This subset displayed a strong positive correlation between transcript and protein abundance ($r = 0.54$, $P = 0.00047$; Figure S9D), and a negative correlation between DHU levels and protein abundance ($r = -0.35$, $P = 0.038$; Figure S9E). These data suggest that DHU is predominantly, but not always, negatively associated with mRNA and protein abundance.

AtDus2 loss-of-function leads to alterations in mRNA stability

Given the observed negative relationship between DHU level and mRNA abundance in both Arabidopsis and Sorghum, we next assessed whether DHU was impacting RNA stability. We first examined differences in global uncapped mRNA profiles between Col-0 and *Atdus2* using the genome-wide uncapped and cleaved transcripts (GMUCT) approach (Gregory et al. 2008; Willmann et al. 2014). In this framework, a higher proportion of uncapped transcripts (GMUCT reads/RNA-seq reads) indicates reduced mRNA stability,

whereas a lower proportion suggests enhanced RNA stability. To assess data quality, we ensured the capture of exon-junction complex footprints in our libraries for both genotypes (Lee et al. 2020, Figure S10A). Using HAMR/Modtect detection, we identified a total of 426 DHU-modified transcripts in Col-0 under control condition, and 302 of these transcripts were associated with reduced DHU levels in the *Atdus2* background (Table S13), suggesting that their DHU status was *AtDUS2* dependent. These DHU-level dependent transcripts were not only more abundant at the transcript level in the *Atdus2* background relative to non-DHU-modified transcripts based on cumulative frequency (Figure S10B, $P < 1e\text{-}16$, solid lines), GMUCT also uncovered a significant reduction in the proportion of uncapped RNAs in the *Atdus2* background relative to Col-0 (Fig. 4a, blue boxplots, $P = 0.00087$). This reduction was not observed for non-DHU-modified transcripts (Fig. 4a, red boxplots, $P = 0.25$), suggesting that the presence of DHU on these transcripts in a Col-0 background was influencing their degradation.

To further test this model, we performed a time course transcriptional arrest experiment, treating 7-d-old Arabidopsis seedlings with the transcription inhibitor cordycepin over a period of 6 hours (Figure S10C). After QC (correlation among replicates > 0.9, alignment rate > 90%) and data normalization based on Sorenson et al. (2018), including the removal of low-abundance transcripts at T_0 and transcripts with high standard error (T_0 average TPM > 8 and SE < 0.5), we retained 12,450 transcripts for modeling using both an exponential regression model (*Exp*) and a nonlinear least squared model (NLS) to estimate the decay rate (K) and half-life (min) for each transcript (Table S14). Using either model, we did not observe a significant change in global RNA decay rates (Table S14). However, when examining just those transcripts for which we could assign DHU status and model decay rates (216/302 transcripts with reduced DHU in *dus2*), we saw both a significant decrease in decay rates and corresponding increase in mRNA half-lives (Fig. 4b**;** left = decay rate, right = half-life estimation). These 216 DHU-modified transcripts could be further divided into 3 groups based on their half-life patterns using clustering as a reference (Fig. 4c and Figure S11A, average half-lives denoted for each cluster), with a great portion all displaying a longer half-life in the *Atdus2* background ($N = 125$; Fig. 4c). Interestingly, these more stable transcripts were predominantly associated with photosynthetic and translation-related GO terms (Figure S11B, top).

We next compared DHU levels, transcript abundance (TPM), and the uncapped mRNA ratio (GMUCT/RNA-seq ratio) among the 3 transcript groups using $\log_2$(dus2/Col-0). Both TPM and the GMUCT/RNA-seq ratio differed significantly among the groups under both conditions ($P < 0.05$; Figure S12A, upper panel), indicating that the extent of degradation between Col-0 and *dus2* varies across these transcripts, in agreement with the transcriptional arrest assay. By contrast, DHU levels did not differ significantly among the 3 groups (Figure S12C**)**. Comparison of DHU site distribution revealed that the group with stronger degradation in Col-0 tended to have DHU sites enriched near the 3′ end of the CDS or within the 3′UTR (Figure S12B). Together, these results suggest that DHU position, rather than its global level, may contribute to mRNA destabilization.

We finally returned to the 38 transcripts for which we saw links between DHU, transcript, and protein abundance (Figure S9D and S9E). Of these, 20 showed both increased transcription and significantly reduced DHU levels in the Atdus2 background ($P = 0.011$; Fig. 4d middle) with 16 out of these 20 displaying significantly increased protein abundance. As expected, these transcripts displayed limited variation in non-DHU RCMs detected by HAMR/Modtect ($P = 0.375$). These differentially DHU-modified transcripts are involved in KEGG-defined metabolic pathways, ribosome function, and photosynthesis-related processes, with most (14/20) localized to either the chloroplast or mitochondria, although these transcripts originate from the nuclear genome (Table S12). A majority of these DHU-modified transcripts with sufficient GMUCT coverage (15/18) also displayed a significant decrease in the proportion of uncapped reads relative to Col-0 ($P = 0.00033$, Fig. 4d middle), suggesting DHU-dependent transcript degradation. Half-life modeling largely agreed with this model of DHU-dependent degradation, as 12/15 transcripts (with sufficient data to model) showed an increased half-life in the Atdus2 background, with half-life estimates increasing by ∼2- to 10 fold for 4 transcripts as displayed (Fig. 4e, full dataset and modeled rates found in Table S14). Thus, under normal growth conditions, DUS2, and the RCM DHU, appear to be important for turnover of a core subset of transcripts associated with photosynthesis and metabolism.

DHU impacts photosynthesis-associated traits under abiotic stress in Arabidopsis

Given SbDUS2's connection to performance under abiotic stress in sorghum, we next sought to validate this role in the context of a *Atdus2* loss-of-function background in Arabidopsis plants. First, we assessed whether there was a DUS2-dependent impact on plant performance under the 2 main stressors sorghum experienced in the field, water deficit and heat stress, applied separately here for Arabidopsis. We monitored vegetative growth and development of Col-0 and *Atdus2* mutants seedling (SALK_079129C and CS857388) under water withholding or heat stress conditions. Water withholding was performed by reducing soil water content (SWC) from 70% (control conditions) down to 25% (drought) over 6 days and then holding SWC at 25% for 3 additional days on 4-week-old seedlings, with images that have been analyzed to estimate approximate growth rates (Fig. 5a). As expected, Col-0 plants displayed reduced rosette area under water withholding conditions, indicating that the stress was successfully applied to these plants (Fig. 5b). Plants lacking *Atdus2* showed a significant ∼50% reduction in rosette area relative to Col-0 under both control and water withholding conditions (Fig. 5b). Heat stress, applied to 2-week-old seedlings for 12 days, resulted in a similar relative decrease in plant growth for both Col-0 and *Atdus2* mutants; however, the *Atdus2* mutant backgrounds showed significantly reduced survival rate at the end of the experiment (Fig. 5c and 5d). Seven-day-old *Atdus2* mutant seedlings showed a similar response when exposed to heat stress for 72 hours (37 °C) on 1/2 MS plates, suggesting this is a robust sensitivity to heat stress.

We next assessed photosynthetic capacity via the LI-6800 system (net CO_2 assimilation) in both the Col-0 and *Atdus2* drought-stressed and heat-stressed plants (Fig. 5e). Interestingly, we observed a slight, but nonsignificant decrease in net CO_2 assimilation under control conditions between *Atdus2* and Col-0, whereas the *Atdus2* background showed a significant reduction under both stress conditions ($P <<< 0.05$ in both treatments; Fig. 5e). As an additional line of evidence, we subjected 2 independent complementation lines (DUS2–3×FLAG-pH7WG2: Line 2–24 and Line 1–2) to the same stress treatments. Under both drought (3-week seedlings) and heat conditions (1-week seedlings), these lines exhibited phenotypes comparable to Col-0, supporting successful functional complementation and further linking DUS2 to the observed stress phenotypes (Fig. 5f).

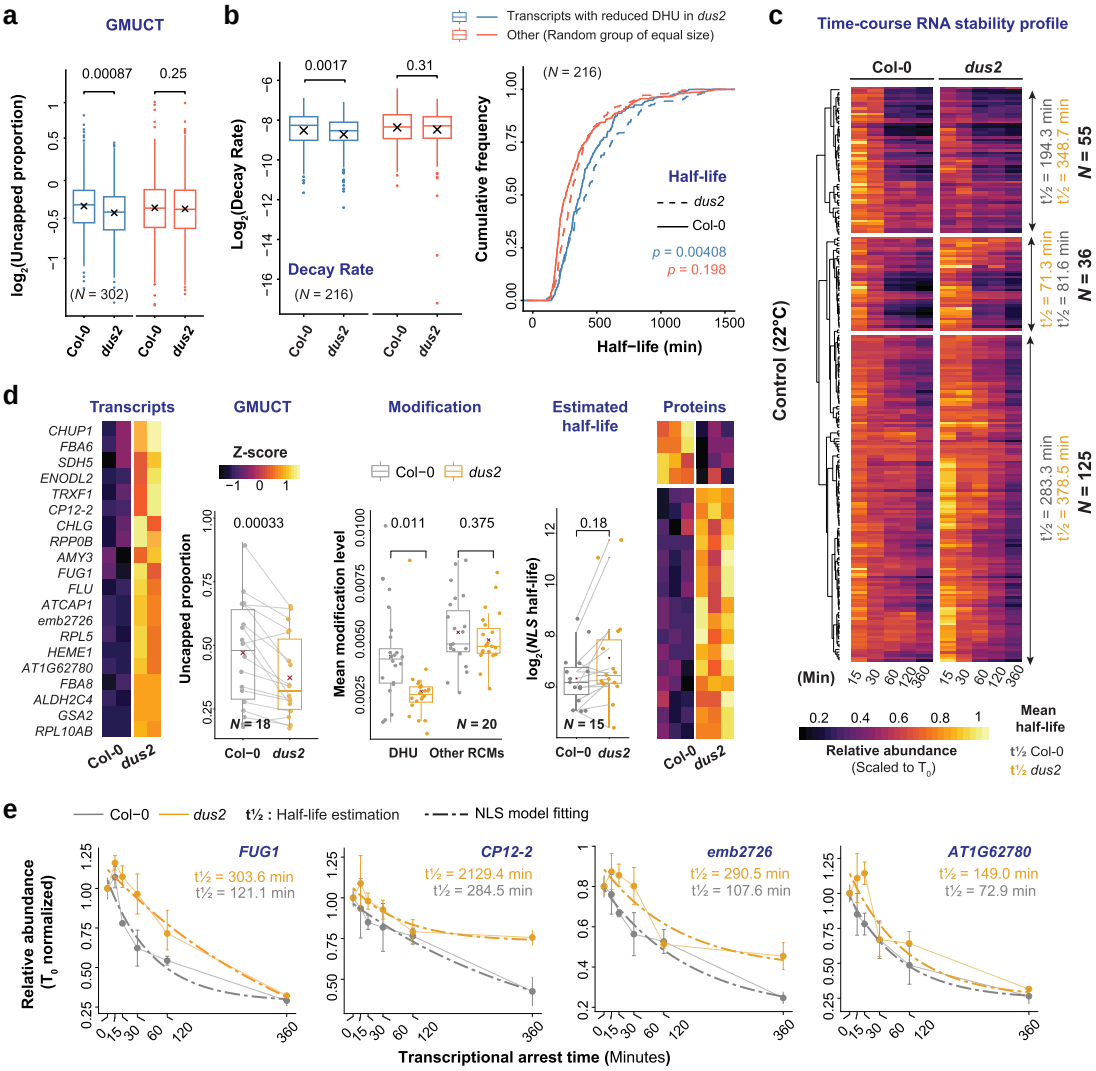

Figure 4 Altered RNA stability between col-0 and *dus2* background. (a) Boxplot shows comparison of GMUCT-derived uncapped portions per transcripts over transcripts associated with lower DHU level in *dus2* and other transcripts in Col-0 and *dus2* background, examinate by Wilcox test. (b) Decay rate (k) on groups of transcripts with lower DHU level in *dus2* mutants were compared with subset of randomly selected transcripts with equal sample size using Student *t* test ($P < 0.05$) on the left; Cumulative frequency of estimated half-life of transcripts in Col-0 (solid line) and *dus2* (dashed line) background with lower DHU level in *dus2* mutants were compared with randomly selected transcripts on the right using Wilcoxon signed-rank test ($P < 0.05$). (c) Heatmaps show differentiated decay rate of transcripts derived from panel (b), which show a majority faster decay in Col-0, partial similar decay between 2 genotypes, and small groups with slower decay in Col-0 under both control and heat conditions. (d) Heatmap of 20 transcripts associated with differential DHU, transcript abundance, and protein abundance was plotted. Boxplots show GMUCT and RNA modification level of 16 transcripts with reduced protein in Col-0 relative to *dus2* (Wilcox test, $P < 0.05$), along with estimated half-life comparison of 14/16 transcripts (Wilcox test). (e) RNA decay curve 6-hour experiment and line graph (error bars displayed) of 4 selected transcripts associated with higher DHU level and faster degradation in Col-0 than *dus2*, with estimated half-life were using NLS model.

These data suggest that AtDUS2, and DHU, is important for full photosynthetic capacity under drought and heat stress.

Heat stress induces pronounced alterations in mRNA stability in Atdus2

Next, we aimed to understand the DHU-dependent molecular responses that make the *Atdus2* background less robust under abiotic stress. For this, we profiled *AtDUS2*-dependent transcripts and DHU abundance, as well as RNA-decay changes that occur in response to heat stress in Arabidopsis. Heat stress, rather than water withholding, was applied, as it is easier to apply consistently and quantitatively and also it can be applied to seedlings in the RNA-decay experimental framework. In addition, our data indicated that *Atdus2* mutants showed diminished growth/survival at both the seedling and vegetative rosette stages under heat stress (Fig. 5). We monitored DHU abundance using HAMR/Modtect RCM calling of Illumina RNA-seq collected daily over a period of 4 days following implementation of heat stress ($N = 8$ per genotype and condition). An examination of these data revealed significantly increased mean DHU levels in Col-0, but not in *Atdus2*, in plants exposed to heat stress relative to their appropriate controls (Fig. 6a, $P = 0.048$ and $P = 0.88$, respectively), suggesting that DHU is a standard mRNA-level stress response. As expected, we also observed a significant heat stress–associated increase in the other

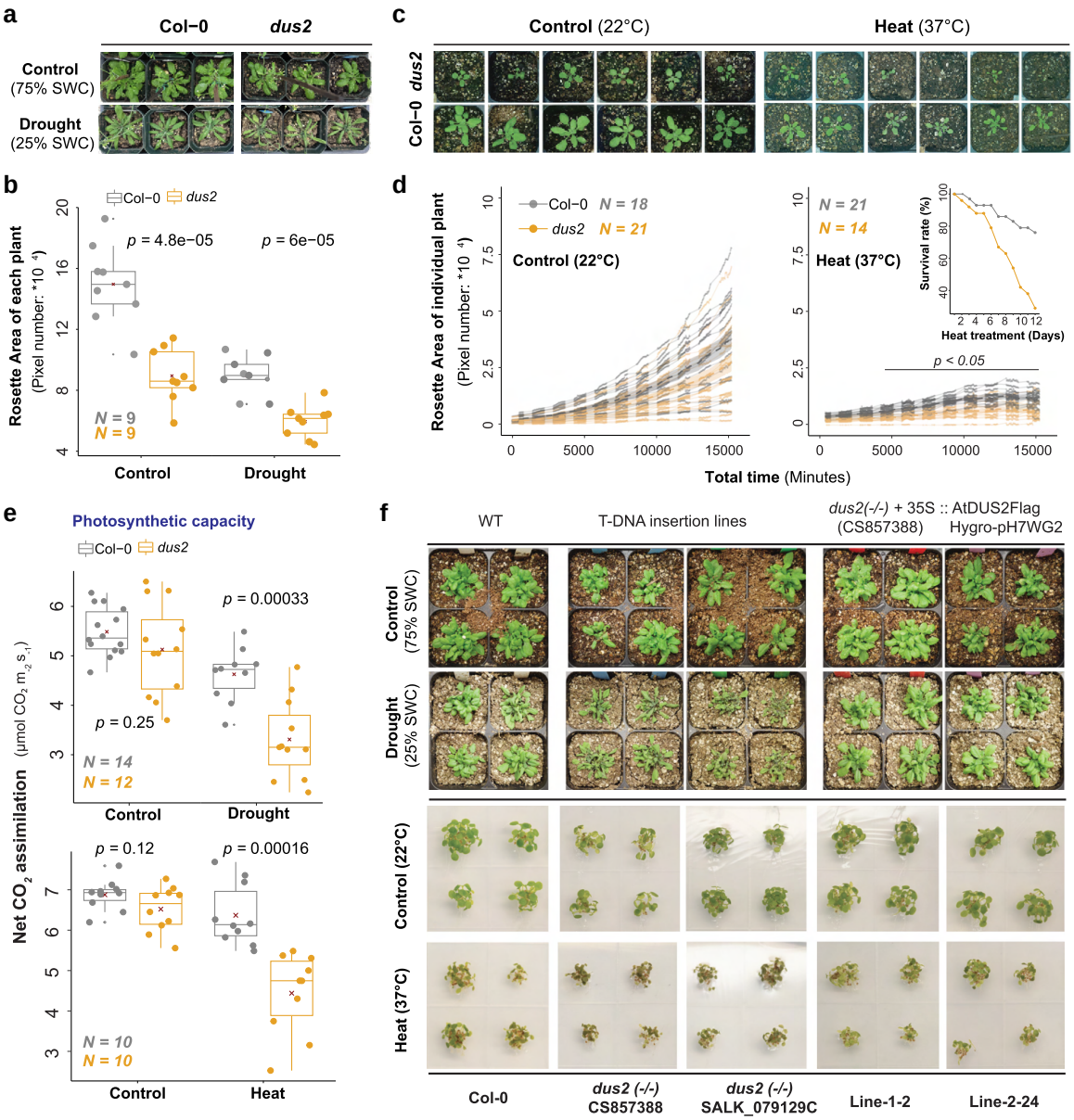

Figure 5 Examination of abiotic stress response between col-0 and *dus2* in Arabidopsis. (a) Arabidopsis rosettes of 4-week-old seedlings of 2 genotypes among control (70% SWC) and drought (25% SWC) conditions were displayed. (b) Comparison of Arabidopsis rosette area at the last day of drought treatment between Col-0 and *dus2* plants under 70% SWC and 25% SWC conditions (Student *t* test, $P < 0.05$). (c) Images show Arabidopsis rosette characteristics at the twelfth day of heat treatment between 2 genotypes. (d) Image-based phenotyping of Arabidopsis rosette area over 12 days of vegetative growth under control and heat conditions (30-minute interval) processed by PlantCV (Yu et al. 2024a) with Student *t* test performed between genotypes ($P < 0.05$). Inset panel under heat depicts survival rates over time. (e) Photosynthetic efficiency (net CO_2 assimilation) was measured on the largest rosette leaf using a LI-6800 system. CO_2 net assimilation rate under heat (24 h at 37 °C) and control (22 °C), control (70% SWC) and drought (25% SWC) were measured with more than 10 replicates per genotype per condition. (f) Phenotypic characterization of Col-0 (WT), 2 *dus2* T-DNA insertion lines (CS857388 and SALK_079129C), and 2 independent DUS2–3×FLAG-pH7WG2 rescue lines under drought (3-week seedlings) and heat conditions (1-week young seedlings).

HAMR/Modtect identifiable RCMs in both Col-0 and *Atdus2* backgrounds (Fig. 6a, $P = 0.037$ and $P = 0.024$, respectively). These data indicate a heat-dependent shift in DHU profiles that is dependent on *AtDUS2*.

We then profiled the transcriptomic changes that occurred in these 2 backgrounds following heat stress. A total of 3,186 and 3,259 transcripts (Table S15) were differentially abundant in Col-0 and *Atdus2*, respectively, between control and heat stress conditions (*FDR* < 0.05, $|\log_2 FC| > 1$; Figure S13A and S13C). As expected, the transcripts upregulated in both backgrounds (Figure S13B, gray bars) were enriched for stress response–related terms, indicating that the applied stress was sufficient to elicit a response However, terms enriched in the set of Col-0 specifically upregulated transcripts suggest that it was mounting a response to DNA damage, recombinational repair, and slowing down cell division, whereas the *Atdus2* mutant exhibited an increase in terms related to jasmonic acid and a decrease in terms related to salicylic acid and photosynthesis (Figure S13D). To elucidate genotypic-specific stress response due to *Atdus2* loss of function,

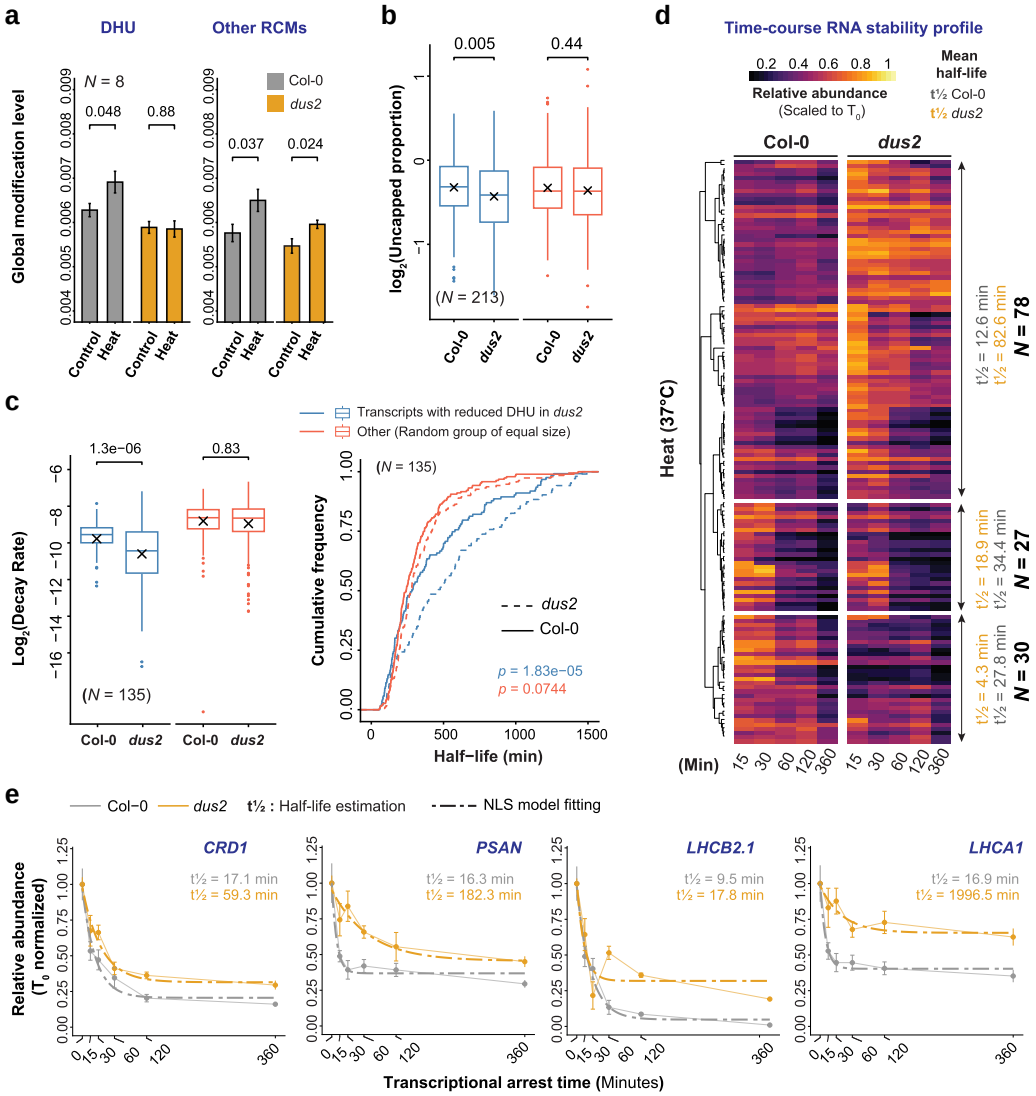

Figure 6 Comparison of abiotic stress-induced RNA stability between col-0 and *dus2*. (a) Global DHU level and modification level of other RCMs were compared between 2 genotypes under both control and heat conditions ($N = 8$), examinate by Student *t* test. (b) Boxplot shows comparison of GMUCT-derived uncapped portions per transcripts over transcripts associated with lower DHU level in *dus2* and other transcripts in Col-0 and *dus2* background under heat conditions, examinate by Wilcox test. (c) Left: Decay rate (k) based on exponential modeling on groups of transcripts with lower DHU level in *dus2* mutants under heat condition was compared with subset of randomly selected transcripts with equal sample size using Student *t* test ($P < 0.05$). Right: Cumulative frequency of estimated half-life of transcripts in Col-0 (solid line) and *dus2* (dashed line) background with lower DHU level in *dus2* mutants were compared with randomly selected transcripts under heat stress using Wilcoxon signed-rank test ($P < 0.05$). (d) Heatmaps show differentiated decay rate of transcripts derived from panel (c), with majority faster decay in Col-0, and 2 small groups with slower decay in Col-0 under heat conditions. (e) RNA decay curve across 6-hour experiment and line graph (error bars displayed) of 4 selected transcripts associated with higher DHU level and faster degradation in Col-0 than *dus2*, with estimated half-life using NLS model.

we profiled the unique transcripts that were differentially abundant in response to heat stress (Figure S10D). Particularly, these are a subset of transcripts that exhibited a strong stress response in the Col-0 but were unaltered in the *Atdus2* background (Figure S10D, red boxes), suggesting that a functional DUS2 was necessary for their heat-associated response. We profiled the top 3 nonredundant KEGG and GO terms of transcripts either up- or downregulated in Col-0 in response to heat (Figure S10D, dashed lines, Table S16). As expected, photosynthesis was the top enriched KEGG and GO term in the downregulated transcripts in Col-0 in response to heat. In sum, these data suggest that Arabidopsis DUS2 is necessary for an appropriate DHU-mediated stress response, with photosynthesis-related traits and transcripts the primary target.

To further explore the mechanism driving the increased stress susceptibility observed in the *Atdus2* background, we next assessed if DHU-associated changes might influence RNA stability during heat stress. To assess RNA stability, 7-day-old seedlings in 1/2 MS liquid culture were acclimated at 37 °C for 12 hours, and then treated with cordycepin, with samples collected over 6 hours as we did under control condition (Figure S10C). Global profiling of mRNA decay rates for the 12,450 model-fitted transcripts (Table S14) revealed that, in response to heat stress, a substantial proportion of mRNAs exhibited longer

half-lives in *Atdus2* compared with Col-0 under both conditions (~47% under control and 51.6% under heat [$\log_2$FC(half-life ratio) > 0.1]; Figure S10E). We then focused on transcripts with detectable DHU in Col-0 under heat stress. Using the HAMR/Modtect approach, we identified a total of 357 DHU-modified transcripts in Col-0 under heat, 213 of which showed reduced DHU in *dus2* and were also associated with higher uncapped reads in transcripts based on GMUCT data (Table S13, Fig. 6b). Further selecting for transcripts with fitted decay models, we obtained 135 transcripts for comparison. For these transcripts, we observed significantly reduced decay rates (K) under heat in the *Atdus2* background ($P = 1.3e-06$, blue boxplots) that was not evident for non-DHU-modified transcripts (red boxplots; Fig. 6c, left, $P = 0.88$). This result is consistent with the cumulative frequency of half-lives, where transcripts associated with reduced DHU level in *Atdus2* exhibited significantly shorter half-lives in Col-0 than *dus2* ($P = 1.83e-05$, blue lines). In contrast, the half-lives of non-DHU-modified transcripts remained unchanged between the 2 genetic backgrounds (Fig. 6c, right, $P = 0.0744$, red lines).

A closer examination of these 135 transcripts using clustering heatmap uncovered 3 groups of transcripts with differentiated decay profiling (Fig. 6d). More than half of transcripts ($N = 78$) exhibited substantially reduced half-lives in Col-0 relative to *Atdus2* in response to heat stress (Fig. 6d and Figure S11A, average half-lives denoted for each cluster), whereas the remaining 57 transcripts exhibited increased half-lives in Col-0 under heat. In control settings, the DHU-modified transcripts with increased half-lives in the *Atdus2* background were enriched for the expected photosynthetic terms ($N = 125$, Figure S11B, top). Photosynthetic terms were also enriched for the pool of 78 DHU-modified transcripts with increased half-lives under heat in the *Atdus2* but were also accompanied by abiotic stress terms (Figure S11B, bottom). Of the 78 DHU-modified transcripts that displayed a longer half-life in the *Atdus2* mutants relative to Col-0 under heat stress, 33 were associated with photosynthesis terms, including common photosystem I and II-associated transcripts, (eg LHCA, LHCB, and PSB transcripts). Indeed, these transcripts had some of the largest half-life shifts, ranging from 2× to 100× longer (Fig. 6e), indicating that DHU is necessary for their faster turnover in Col-0. We then compared the TPM, DHU levels, and uncapped RNA levels (ie GMUCT ratio) among the 3 groups of transcripts. Consistent with the results under control conditions, DHU levels under heat stress did not appear to be the primary factor underlying the differences in transcript abundance [log2(dus2/Col-0), TPM] or uncapped read ratio [log2(dus2/Col-0), GMUCT] among 3 groups of transcripts with reduced DHU in the mutant. Rather, DHU deposition near the 3′ end of the CDS or within the 3′UTR appears to be associated with the faster mRNA decay observed in Col-0 relative to *dus2* (Figure S12, bottom). In sum, these data suggest that the diminished performance under heat stress is likely due to impaired turnover of these photosynthesis-related transcripts and point to a post-transcriptional regulatory mechanism for these critical genes.

Discussion

Drought and heat are common abiotic stressors that induce complex phenotypic and molecular responses that often lead to reduced photosynthesis, biomass, and seed set, thereby adversely affecting the overall productivity of agricultural crops. Sorghum's adaptation to heat and drought makes its genetic and phenotypic diversity useful for revealing regulatory mechanisms that enable maximal growth under diverse field conditions. Although a variety of stress-responsive genes have been identified in sorghum and other stress-resilient plant species (Pardo and VanBuren 2021; Pardo et al. 2023), gaps remain, particularly in post-transcriptional regulatory events that have been shown to impact performance in other species.

To connect differences in plant performance in the field to specific transcriptional and post-transcriptional regulatory events, we performed a multi-omic comparison of 6 diverse sorghum accessions grown under water-limiting and control conditions. We integrated molecular and physiological variation in a systems-level analysis to identify potential causal factors. As expected, physiological parameters and genes associated with photosynthesis, water movement, and stress-response regulation were all impacted to varying degrees in our panel (Fig. 1). Interestingly, we also observed variation in one of the RCMs that we were able to detect through standard Illumina RNA-sequencing approaches, DHU, that was strongly correlated with transcript abundance and plant performance in the 6 accessions (Fig. 2a). Furthermore, our co-expression network analysis identified a dihydrouridine synthase (*SbDUS2*) transcript that was also associated with photosynthesis traits and DHU status of related transcripts. Importantly, the correlation between *SbDUS2* expression and the suite of transcripts with predicted DHU sites was observed in other public datasets and was not unique to our specific field conditions, growth parameters, or accessions. Thus, SbDUS2 and DHU appear to be linked with transcript groups associated with physiological traits.

While RCMs have been shown to influence or be associated with plant stress responses (Yu et al. 2021; Sharma et al. 2023; Cai et al. 2025), the identification of SbDUS2 associated with photosynthesis and stress-related transcripts was nevertheless a surprise. The DHU modification is mostly associated with tRNAs, including in plants (Chen et al. 2010; Brégeon et al. 2022; Ju et al. 2025), and indeed the DUS protein family is conserved across the tree of life, including in eukaryotes, prokaryotes, and some archaea (Yu et al. 2011; Finet et al. 2022a, 2022b). Due to advances in detection capabilities, DHU has recently been described on mRNAs in humans and yeast (Dai et al. 2021; Draycott et al. 2022; Finet et al. 2022a; Ju et al. 2025), where it has been reported to influence splicing, translation, and fundamental biological processes such as meiosis (Finet et al. 2022a). Using computational algorithms that infer DHU status based on nonrandom errors introduced during the RT-PCR step of RNA-seq library preparation, we were also able to predict DHU-marked transcripts, and indeed our data suggest that these transcripts were enriched for a set of photosynthesis, metabolism, and other fundamental cellular processes. Whether this is due to sequence intrinsic features, functional conservation, or speculatively is an ancient organellar feature from before they were incorporated into the nuclear genome, is unclear and will likely guide future discoveries. The apparent enrichment of predicted DHU among highly abundant transcripts likely reflects, at least in part, an abundance-dependent detection bias, as the sensitivity of DHU calling increases with read depth (Figure S4B and S4C). Higher resolution transcript-level profiling of DHU, especially in low-abundance transcripts, will likely depend on further technical advances, such as improved direct RNA-seq platforms and detection algorithms, or approaches that leverage the intrinsic chemical reactivity of DHU for transcriptome-wide mapping (Draycott et al. 2022; Finet et al. 2022a; Ju et al. 2025).

Given this detailed study of DHU in plants, and in particular on how DHU might contribute to plant growth and development, we sought to develop a clearer picture of how DHU is performing this function by

examining Arabidopsis lines with the orthologous *Dus2* locus disrupted. Since we expected much of this DHU signal to be associated with the more abundant tRNA class, we also specifically examined mRNA-enriched and tRNA-associated DHU levels using LC-MS/MS, as well as 2 sequencing-based approaches (Modtect/HAMR and DRS) between WT (Col-0) and *Atdus2* mutants (Fig. 3B and 3c). We observed a DUS2-dependent decrease in DHU levels in mRNA using these complementary approaches, suggesting that AtDUS2, like other eukaryotic DUS2 enzymes, modifies mRNAs in addition to other RNA classes. With evidence supporting a DUS2-dependent reduction in mRNA-associated DHU, we then assessed the impact that diminished DHU abundance had on plant performance. A real concern is that loss of *AtDus2* could have pleiotropic effects on plant performance through impaired nuclear or chloroplast-encoded tRNA modification. LC-MS/MS, ModTect/HAMR, and DRS demonstrated that that DHU was reduced in both purified tRNA and rRNA-enriched RNA and was reduced and reprogrammed in mRNA in the Arabidopsis *dus2* background (Fig. 3b). However, untargeted proteomic profiling did not reveal a global reduction in protein abundance (Figure S9), instead it showed more specific decreases in proteins associated with photosynthesis and metabolism, consistent with the functional classes enriched among DHU-associated mRNAs. Nor did we observe a broad change in chloroplast-encoded proteins, as would be expected if DUS2 acted in a similar manner to previously identified chloroplast-localized tRNA-modifying enzymes in rice (Liu et al. 2020). Together, these results suggest that the phenotypic and transcriptomic changes in *dus2* are unlikely to be explained solely by broad defects in translation.

A central question for mRNA DHU, as for other RNA chemical modifications, is whether it affects transcript stability. By combining global transcriptional arrest and GMUCT analyses, we obtained complementary lines of evidence that DHU in mRNAs is associated predominantly with transcript destabilization, reflected by altered half-lives in a subset of transcripts enriched for metabolic and photosynthetic functions (Fig. 4). This observation is also supported by the known biochemical properties of DHU, which introduces marked structural changes to uridine, disrupts base stacking, alters sugar pucker conformation, and increases local RNA flexibility, thereby reducing thermodynamic stability (Sipa et al. 2007; Draycott et al. 2022). While the precise molecular mechanism remains unresolved, these properties suggest that DHU could reshape local mRNA structure or accessibility and, in turn, influence interactions with ribosomes, RNA-binding proteins, or components of the RNA decay machinery.

The observed impact of *AtDus2*-dependent DHU on photosynthesis was more pronounced under abiotic stress conditions in Arabidopsis, with reduced *AtDUS2* levels associated with decreased plant performance. This raises the question of how a modification that appears to be negatively associated with transcript abundance could be beneficial for plant performance under stress? We propose a model, supported by RNA decay data in both Col-0 and *Atdus2* mutants under control and heat conditions, whereby DHU is likely necessary for appropriate mRNA turnover under stress conditions (Fig. 7). The observation that DHU-associated photosynthesis transcripts, which inhabit several layers of the core photosynthesis process, from chlorophyll biogenesis to carbon fixation, exhibited substantially increased half-lives (up to 100-fold) in the *Atdus2* background provides support for our model of DHU-dependent transcript destabilization. In addition, prior work examining HAMR-detectable RCMs in Arabidopsis found that this group of modifications, which included DHU, were heavily enriched on actively degrading transcripts under control conditions (Vandivier et al. 2015). Higher turnover, reduced steady state levels, and structural perturbations of photosynthesis- and metabolism-related transcripts have been observed under stress conditions in a number of plant systems (Li et al. 2022; Notarnicola et al. 2025) with these changes proposed as a rapid means of clearing molecules that are accumulating damage caused by reactive oxygen species (ROS; Park et al. 2012). While plants attempt to limit photosynthesis during stress, as it is one of the main ROS-producing mechanisms in the cell, inappropriately elevated photosynthesis can lead to cell death–inducing ROS levels. We propose that DHU is an RCM that marks mRNAs for degradation, thereby helping to clear them more rapidly and facilitate a proper response to environmental perturbations. Whether this occurs co-transcriptionally in the nucleus or post-transcriptionally in the cytoplasm remains to be determined. Excitingly, there is a clear connection between the cytoplasmic mRNA decay machinery and stress tolerance in Arabidopsis (Merret et al. 2013) and DHU, or a sufficient accumulation of DHU marks, may target mRNAs toward this pathway. We propose that Arabidopsis plants lacking DUS2, or that decrease DUS2 levels or activity in response to stress conditions, would then be unable to clear these damaged mRNA molecules through cytoplasmic decay pathways, potentially increasing cell death and diminishing plant performance.

In summary, our comparative, multi-species approach facilitated the identification of an RCM that appears to be critical for plant performance under stress. Indeed, this RCM influences abiotic stress responses in Arabidopsis by acting on many of the photosynthesis-related and metabolism-related mRNAs. These data highlight the complex transcriptional and post-transcriptional regulatory landscape influencing plant stress responses and offer promising insights as to how they might be used to select more stress-resilient plants in the future.

Materials and methods

Sorghum growth and phenotypic measurement

Six selected sorghum accessions (PI 533871: M1, PI 533961: DL/59/1530, PI 656041: 80M, PI 656053: N290-B, PI 656076: SC1271, and PI 656096: SC391) were grown at the University of Arizona Maricopa Agricultural Center. All plants were well-watered (WW) at the same rate (~24% soil volume metric water content, SVWC), corresponding approximately to the soil field capacity) until flag leaf appearance in the whorl (~47 days after planting), after which irrigation was reduced to a subset of plots to mimic drought treatment (water-limited, WL; 16% SVWC). The destructive plant phenotyping was conducted at the end of the season (maturity stage). Measured traits included above-ground biomass, root biomass, and 3-leaf weights. For other time-series molecular phenotypes, samples were collected weekly (on Thursdays) for 7 weeks (week 1–week 7, from August 13 to September 24, 2020) on a specific range of a large field experiment conducted at the University of Arizona's Maricopa Agricultural Center. For transcriptomics, metabolomics, and analysis of other biochemical traits, samples consisting of 6 leaf disks from 5 different plants per accession, treatment, and time point were collected (from 10:30 to 11:30) in 3 different 1.5 mL tubes and immediately snap-frozen in liquid nitrogen (plot level replicates = 2). LI-6800 derived photosynthesis-related traits ($N = 29$, replicates = 5, LI-COR Lincoln, NE) were measured in the morning (from 9:00 to 10:00) and afternoon

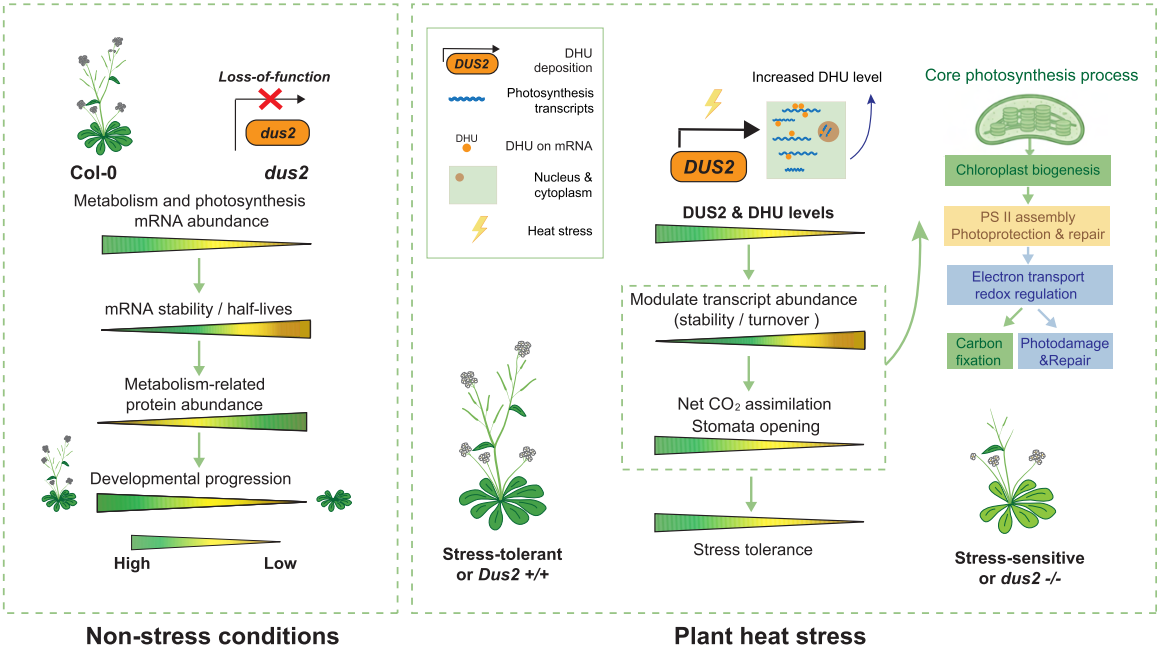

Figure 7 Proposed model explains DHU impacts on plant growth and stress response. Based on our findings in *Arabidopsis*, reduced DHU levels appear to impact the abundance of a subset of DHU-modified transcripts in Col-0. Loss of DUS2 shifts the stability and half-lives of mRNAs encoding proteins involved in photosynthesis and metabolism, which in turn leads to impaired germination and delayed growth in the mutant background. Growth defects are exacerbated when plants are grown under abiotic stress conditions, due to a proposed inappropriate turnover of photosynthesis-associated transcripts. Counterintuitively, increases in these unmodified photosynthesis-related transcripts in the *Atdus2* mutant leads to reduced photosynthesis parameters, likely due to a buildup of ROS and eventual cell death. Thus, DHU is necessary to reduce mRNA steady state levels, or to target mRNAs for degradation, helping to manage the pool of photosynthesis-related proteins and ultimately allowing for better stress tolerance.

(from 13:00 to 14:00) with the following settings: Flow rate = 600 µmol s^{-1}; Mixing fan speed =12,000 rpm; CO_2 = 420 ppm; Light = 2,000 µmol m^{-2} s^{-1}. The youngest fully expanded leaf on the main stem of each plant was selected for the measurements and data were logged as soon as assimilation and stomatal conductance curves (monitored in real-time on the instrument display) when reaching a plateau (on average 30 seconds after a leaf was clamped).

Sorghum biochemical trait measurements

Highly concentrated metabolites and levels of oxidative stress-related markers or enzymes with 5 replicates per sample were analyzed using an existing protocol (Melandri et al. 2020). Chlorophyll and carotenoid contents were measured after acetone extraction (Porra et al. 1989). Sugar levels were quantified using enzyme-coupled assays (Riewe et al. 2012). Oxidative stress markers, such as malondialdehyde (MDA) and protein carbonyl content, were measured to assess lipid peroxidation and protein oxidation (Levine et al. 1994; Hodges et al. 1999). Photorespiration-related enzyme activities, glycolate oxidase (GOX) and hydroxypyruvate reductase (HPR), were assessed based on established methodologies (Feierabend and Beevers 1972; Schwitzguebel and Siegenthaler 1984). Lipoxygenase (LOX) was extracted in potassium phosphate buffer (pH 7.0), and its activity was measured by changes in conjugated dienes. Total antioxidant capacity (TAC), total polyphenol content (Poly), and flavonoids were evaluated using standard spectrophotometric assays (Benzie and Strain 1999; Zhang et al. 2006b). Enzyme activities of key antioxidants, including ascorbate peroxidase (APX), dehydroascorbate reductase (DHAR), monodehydroascorbate reductase (MDHAR), glutathione reductase (GR), peroxidase (POX), superoxide dismutase (SOD), glutathione peroxidase (GPX), catalase (CAT), ascorbate oxidase (AO), and glutathione *S*-transferase (GST), were determined using microplate-based kinetic assays (Aebi 1984; Murshed et al. 2008).

Sorghum metabolite profiling

Primary sorghum metabolites with 5 replicates per sample were quantified using GC-MS (Wase et al. 2022). Briefly, metabolites were extracted by methanol: water: chloroform solution from 30 ± 3 mg fresh weight (FW) of frozen samples. Ribitol was added to the extraction solution as internal standard. Dried metabolites were derivatized by methoxyamination and trimethylsilylation and analyzed by a 7200 GC-QTOF system (Agilent, St Clara, CA, USA) using a HP-5MS-UI column (30 m 0.25 mm ID 0.25 µm; Agilent) with 100× split and splitless modes. Metabolite peaks were annotated by MassHunter Analysis (Agilent) using the Fiehn Metabolomics Library (Agilent). The 42 most confidently annotated metabolites were quantified by MassHunter Quantitation (Agilent), and the peak heights were background subtracted and normalized by internal standard and precise fresh weight of the sample to calculate the relative metabolite contents values.

General characterization of the Arabidopsis *dus2* mutants

Arabidopsis Col-0 and *dus2* mutant lines (Line ID: CS857388 and SALK_063052C, https://abrc.osu.edu) were grown under standard Arabidopsis long-day conditions unless otherwise specified (22 °C, 60% humidity, and 16 h light, 8 h dark). All seeds were stratified at

4 °C for 48~72 hours prior to planting. T-DNA insertions were confirmed by PCR using primers designed from Salk T-DNA Express (http://signal.salk.edu/tdnaprimers.2.html; SALK_063052-LP: GATTGAGCTGGAACGTCTCAC, SALK_063052-RP:AGCAGAATCTGAGAACCAAATG; SALK_063052-BP(LBb1.3):TATTTTGCCGATTT

CGGAAC; CS857388-LP: ACGCTCTCTTTCAGGATGTTG, CS857388-RP: GCTGGTACACCAAGTTT

CTCG, CS857388-BP(L4): TGATCCATGTAGATTTCCCGGACATGAAG). PCR was performed for 40 cycles with an annealing temperature of 56 °C. Germination assays were performed on 1/2 MS medium with Col-0 and *dus2* mutant seeds at 22 °C during each 3-hour interval for 27 hours after seed stratification (Murashige and Skoog 1962). Two weeks after germination, Col-0 and *dus2* mutant accessions were divided into separate batches for plant growth rate (kept under long-day conditions) and photosynthetic measurements (shifted to a short-day chamber). Four weeks after germination, abiotic stress treatments were applied.

Plasmid construction, plant transformation, and Western blotting

To generate the AtDUS2–3×FLAG-pH7WG2 construct for complementation, the 1,073-bp AtDUS2 coding sequence (with 3 copies of the FLAG epitope at the 3′/C-terminus) was amplified and cloned into the pH7WG2 vector (https://vectorvault.vib.be/plasmid-information) via In-Fusion cloning (Takara Biosciences: 639650), placing the transgene under the control of the CaMV 35S promoter found within the pH7WG2 vector. The AtDUS2–3×FLAG-pH7WG2 construct was introduced into *dus2* (CS857388, –/–) mutant plants by *Agrobacterium*-mediated transformation using the floral dip method (Zhang et al. 2006a). Transgenic lines were placed on 1/2 MS medium containing 20 mg/L hygromycin for selection, following positive transformants confirmation using gene-specific primers for PCR amplification (LP: TTTACTATTCTAGTCGACCTGCAG; RP: TTTTGCGGACTCTAGCATGG; Tm: 59 °C, 40 cycles). Two independent transformants and their offspring were used to assess complementation. For immunoblot analysis, total protein was extracted in Laemmli SDS sample buffer (pH 6.8) containing Tris-HCl, SDS, glycerol, 2-mercaptoethanol, and bromophenol blue. Equal volumes of protein extracts were separated on a 10% SDS–polyacrylamide gel and transferred to a membrane. FLAG-tagged proteins were detected using mouse anti-FLAG monoclonal antibody (MilliporeSigma, F1804; 1:1000) overnight at 4 °C, followed by goat anti-mouse HRP-conjugated secondary antibody (Invitrogen, 31430; 1:10,000) for 2 hours at room temperature. Westerns were developed using Clarity Western ECL substrate (Bio-Rad, 1705060).

Measuring impact of abiotic stress on growth rates of Arabidopsis *dus2* mutants

Arabidopsis Col-0, 2 *dus2* mutant lines (CS857388 and SALK_063052C), and 2 complementation lines (AtDUS2–3×FLAG-pH7WG2: Line 2–21 and Line 1–2) were used for abiotic stress experiments. Drought treatment occurred at 22 °C, with soil water content (SWC) held at 75% for control and 25% for drought set, and lighting period: 8:00 to 21:00 for 3 days on 4-week-old seedlings. Leaf area measurements (Col-0 and CS8573880) were performed using RGB images after a 6-day water withholding period on plant rosettes (replicates = 9) using the PlantCV pipeline for trait extraction (Fahlgren et al. 2015). Heat treatment was performed at 37 °C for plants grown on soil and media plates. For soil seedlings, 2-week-old seedlings were placed under 22 °C and 37 °C conditions over 12 days (replicate > 10). Plant time-series biomass profiling heat and control conditions (Col-0 and CS8573880) were performed using Raspi-controlled phenotyping tools (Yu et al. 2024a) to collect time-series plant RGB images (imaging-interval: 30 mins, length: 12 days) with quantification of digital biomass. For media plate seedlings, 7-day-old seedlings were placed under 22 °C and 37 °C conditions over 72 hours for observation of seedling color with images.

Measuring photosynthetic efficiency in Arabidopsis *dus2* mutants under abiotic stress

The photosynthetic efficiency of *dus2* (CS8573880) and Col-0 lines was evaluated using a gas exchange approach with the LI-6800 (LI-COR Lincoln, NE) with at least 10 replicates for each genotype. Briefly, plants were maintained under short-day growth conditions (photoperiod: 8:00–17:00, temp: 22 °C) to enlarge rosette area to cover the 2-cm^2 small chamber of the LI-6800 device (Brazel et al. 2025). After 4 weeks, plants were kept at 22 °C (control), heat (37 °C for 24 hours), and drought (25% SWC for 24 hours) conditions for gas exchange measurement. Parameters were set as follows: flow rate = 400 µmol s^{-1}; relative humidity of air = 55%-60 %; reference CO_2 = 400 µmol^{-1}; mixing fan speed = 10,000 rpm; heat exchanger temperature: 22 °C or 37 °C; chamber pressure = 0.2 kPa; light source composition 90 % red, 10 % blue light; light intensity = 1000 µmol m^{-2} s^{-1}; and measurement time between 12:00 and 14:00 (Brazel et al. 2025).

RNA extraction and library construction

RNA extraction was performed using methods from previous studies for both Arabidopsis and sorghum (Burgess 2023). Approximately 5 flash-frozen ¼-inch sorghum leaf disks per sample were used as starting material for RNA extractions. RNA extraction was performed using the RNeasy Plant Mini kit (Qiagen #74904) and RNase-free DNase set (Qiagen #79254). Approximately 2.5 to 10 µg total RNA was used as starting material for mRNA enrichment using the Dynabeads mRNA purification kit (Invitrogen, 61006), except with the addition of a second binding and elution step to further enrich mRNA. RNA-seq libraries were then constructed from 10 to 60 ng mRNA per sample using the Amaryllis Nucleics YourSeq Duet Full Transcript library prep kit with combinatorial dual indexes (now Active Motif #23001 or #23002) according to manufacturer instructions. Prepared libraries were sequenced by Novogene with Illumina NextSeq 500 (PE × 150 bp). Arabidopsis RNA was also extracted using Qiagen's RNeasy kit, per manufacturer's protocol. Total Arabidopsis RNA was sent to Novogene for mRNA-enrichment and library preparation, then sequenced on Novogene's NovaSeq X Plus series (PE ×150 bp).

GMUCT sequencing and RNA stability measurement

GMUCT libraries were prepared as previously described (Willmann et al. 2014) using approximately 10 µg of total RNA isolated from the same leaf tissue used for RNA-seq. GMUCT data analysis was performed as previously described (Ganguly et al. 2025), and quality-controlled by ensuring the presence of exon-junction complex footprints in our data. Both RNA-seq reads and GMUCT reads were

processed (replicates = 2) with Hisat2 for mapping and EdgeR to generate reads-per-million–normalized counts (Kim et al. 2019; Chen et al. 2025). The mRNA degradation assay was performed as described (Jia and Le, 2020). Briefly, 7-day-old *Arabidopsis* seedlings of Col-0 and *dus2* were transferred from 1/2 MS solid medium to 1/2 MS liquid medium in 12-well culture plates and incubated for 12 hours at 22 °C (control: 8 hours) or 37 °C (heat treatment: 8 hours). Transcriptional inhibitor cordycepin (final concentration = 0.6 mM; Sigma-Aldrich, C3394) was then added to each well for transcriptional arrest. Tissues (~10 seedlings per biological replicate *3) were collected at 0 min, 15 min, 30 min, 1 h, 2 h, and 6 h after cordycepin treatment for RNA extraction. After the same process of RNA-seq data using Hisat2 alignment and Feature Count pipeline as mentioned above (Liao et al. 2014; Kim et al. 2019), normalization of decay assay was followed as described (Sorenson et al. 2018). Briefly, read counts per gene were normalized based on library size and scaled to 1 million (reads per million), further scaled using 30 stable transcripts-derived RNA decay factor to reflect the fact of decreasing total mRNA in the pool during transcriptional arrest (https://rdrr.io/github/reedssorenson/RNAdecay/f/). Decay rate (K) and mRNA half-life were calculated using exponential regression model $y(t)=Ae^{-kt}$, $t_{1/2}=\ln 2/k$ (A: T_0 normalized abundance, K: decay rate, $t_{1/2}$: half-life) and nonlinear least square model $y(t)=Ae^{-k}t+C$, half-life: $t_{1/2}= -1/k*\ln(0.5\text{-}C)/A)$ (A: T_0 normalized abundance, K: decay rate, $t_{1/2}$: half-life, C: residue) based on in-house R scripts.

5,6-dihydrouridine quantification using LC-MS/MS

Total RNA was extracted from 1 g of Arabidopsis fresh leaf tissue using TRIzol, following the manufacturer's protocol. RNA was quantified and poly(A)+ mRNA was enriched using the Dynabead mRNA Purification Kit (Invitrogen, 61006). The purified mRNA was quality-checked on an Agilent 5200 Fragment Analyzer to confirm depletion of rRNA and tRNA (https://www.agilent.com/en). Purified mRNA (~2 µg) and tRNA/RNA supernatants (~2 µg) was digested to nucleosides using Nuclease PI (0.6 U, Sigma-Aldrich, N8630), phosphodiesterase I (0.2 U, Worthington), FastAP (2 U, ThermoFisher, EF0654), benzonase (10 U, Sigma-Aldrich, E1014–5KU), and pentostatin (200 ng, Fisher Scientific, 20–331-0) in 25 mM ammonium acetate buffer (pH 7.5, ThermoFisher, AM9070G). Reactions were incubated in 100 µL/1 µg RNA overnight at 37 °C and stored at −80 °C prior to LC-MS/MS. Digestion enzymes were removed by 75% MeOH precipitation and centrifugation (21,000 × *g*, 10 min); the supernatant was dried and reconstituted in HPLC-grade water. LC-MS/MS was performed on a Waters Acquity UPLC system coupled to a Xevo TQ-XS triple quadrupole mass spectrometer using an HSS-T3 Premier column (1.8 µm, 100 × 2.1 mm). Mobile phases were water + 0.1% formic acid (A) and acetonitrile (B), run with a standard gradient at 0.3 mL min^{-1}. Dihydrouridine was monitored in positive ESI mode (MRM, 247 → 114.9 m/z) with capillary voltage 1 kV, cone 40 V, and desolvation 400 °C. DHU quantification was based on peak areas relative to an external calibration curve generated with a 5,6-dihydrouridine standard (AdooQ Bioscience, A18909), and absolute DHU abundance was estimated after normalization to sample concentration. In addition, the canonical nucleosides (A, C, G, and U) were quantified in each sample to account for variation in sample loading. Relative DHU levels were normalized as DHU/(A + C + G + U) and compared between Col-0 and *dus2* using Student's *t* test with 5 replicates for each genotype.

Identification and characterization of DHU

Identification of RCMs was performed by intersecting results derived from the High-throughput Annotation of Modified Ribonucleotides (HAMR v1.4) and ModTect (v1.1.5.1) algorithms for sorghum RNA-seq data (Vandivier et al. 2015; Tan et al. 2021). Initially, the paired-end stranded RNA reads were trimmed by Trimmonmatic (v0.32, parameter: TruSeq3-PE.fa:2:30:10:2) to remove adaptors and low-quality reads (Bolger et al. 2014). For HAMR, the forward and reverse reads were mapped to the sorghum reference genome (v3.1.1) using Tophat2 (v2.1.1, –read-mismatches 12 –read-edit-dist 12, –max-hits 10, –lib fr-second strand) (Kim et al. 2013; McCormick et al. 2018), followed by the merging of mapped, removal of multiple-mapped reads, and resolving of splicing alignment using Picard (v3.1.1) and GATK (v3.3.5, (McKenna et al. 2010). Detection were further processed by HAMR with a stringent parameter setting: -min_read_qual 30, -min_read_coverage 50, -hypothesis H_4, -max_FDR 0.05, which filtered out potential modified sites with a < 50 mapping depth with high-confidence (*FDR* < 0.05) to call modified sites (Vandivier et al. 2015). For ModTect prediction, trimmed reads were mapped to the sorghum genome and associated annotation files using STAR v 2.7.10b, (Dobin and Gingeras 2015) with the default arguments and ModTect with the following arguments: -minBaseQual 30, -readlength 150. Only the overlapped sites derived from 2 replicates and 2 methods were retained as the modified sites for each sorghum sample. The type of RCMs was further classified using a XGBoost-based machine learning model (Palos et al. 2024). The output file of Modtech or HAMR was cross-referenced to the gene annotation files to assign sites to transcripts. Here, the ratio of modified reads over total mapped reads per transcript was calculated as RCM level. Location of DHU sites in sorghum and Arabidopsis dataset were generated following workflow of MetaPlotR (https://github.com/olarerin/metaPlotR). The ±1pb flanking regions of each DHU site were harvested to calculate the portions of 3nt motifs around DHU sites.

Population-level genomic analyses in sorghum

Orthologs between Arabidopsis and sorghum were searched based on phytozome12 annotation and confirmed using CoGeBlast (https://genomevolution.org/coge/CoGeBlast.pl, parameters E-value: 1e-5, word_size: 3, matrix: BLOSUM62, TAIR 11 and Sbicolor_454.v3, (Cheng et al. 2017; McCormick et al. 2018). The genomic variants of the 6 sorghum accessions were identified and annotated using sorghum Association Panel (SAP) data (Boatwright et al. 2022). Briefly, trimmed DNA reads were mapped to the sorghum reference genome (BWA-mem: v0.7.17-r1188, (Li, 2013). Duplicated read-pairs and low-quality mapping in each sample were cleaned using Sambamba (Tarasov et al. 2015) (v1.28.1, mapping_quality ≥1 and not (unmapped or secondary_alignment) and not ([XA]! = null or [SA]! = null). Variant calling was conducted using the GATK4 HaplotypeCaller function (v4.2.5.00, parameters: -max-alternate-allele:6, –Ploidy:2, (McKenna et al. 2010). The single nucleotide polymorphisms (SNPs) were filtered using GATK hard-filtering (https://gatk.broadinstitute.org). Those high-quality variants were further annotated by variants effect predictor (VEP) using the *S. bicolor* Sbicolor_454.v3 gene annotation (McLaren et al. 2016). For phylogenetic analysis, we retained the bi-allelic SNPs at the 4-fold degenerate (4DTV) loci filtered by plink (v1.90b4, –types SNPs -m 2 -M 2) that derived from 365 out of 407 sorghum accessions with complete geographical information (Boatwright et al. 2022). Using the SNP filtering with minor allele

frequency (MAF > 0.05, missing data < 0.1) and linkage disequilibrium (LD) prune (plink v1.90b4 parameter: –indep-pairwise 1000 500 0.2, (Purcell et al. 2007), a total of 7,520 SNPs were kept to reconstruct the phylogenetic tree using IQtree (v1.6.12, Parameter: -nt 100 -m MFP, (Nguyen et al. 2015).

Transcriptome data processing

All RNA-seq reads were trimmed using trimgalore (v0.6.10, -paired, -length 10) and mapped to respective reference genomes using Hisat2 (v2.1.0, default setting, (Krueger 2015; Kim et al. 2019). FeatureCounts was used for reads quantification (v2.0.1, parameter: -s 1 -p -t mRNA -g ID -O) and further normalized using DESeq2 after the removal of transcripts with less than an average of one count across samples (Liao et al. 2014; Love et al. 2014). For sorghum, time point, accession IDs, and watering conditions were incorporated as the experimental design factors. In Arabidopsis with Condition (Control and Heat) and genotype (Col-0 and *dus2*) included for experimental design Condition-wise differentially abundant transcripts (DATs) over each time point per accession were identified using the cutoff of false discovery rate (*FDR* < 0.05). A $\log_2$-transformed fold change (FC) > 1 or < −1was used to filter up (down)-regulated transcripts downregulated transcripts. Z-score (row-based) normalization was performed to visualize sample-wise heatmap. TPM (transcripts per kilobase million) were used for comparison of transcript abundance across samples for all transcripts.

Proteomic data processing

Proteolytic digestion

Protein pellets were resuspended in 100 mM Tris-HCl buffer (pH 8.5) containing 4% (w/v) sodium deoxycholate. Proteins were reduced with 10 mM TCEP and alkylated with 40 mM chloroacetamide, then incubated at 45 °C for 5 min with shaking (2,000 rpm). Trypsin (in 50 mM ammonium bicarbonate) was added at a 1:100 enzyme-to-protein ratio (w/w), and digestion was carried out overnight at (37 °C with 1,500 rpm). After digestion, SDC was removed by phase extraction. Samples were acidified to 1% trifluoroacetic acid and desalted. Peptide concentrations were measured using the Pierce Quantitative Colorimetric Peptide Assay Kit (#23275) following the manufacturer's instructions.

LC-MS/MS for data-independent acquisition samples

For DIA analysis, ~200 ng samples (3 replicates each sample) were made onto a RSLC column and washed for 5 min with buffer A (www.thermo.com). Bound peptides were then eluted over 35 min onto a RSLC-resolving column (gradient: 5% B to 38% B). After the gradient, the column was washed with 90% B for the duration of the run (Buffer A = 99.9% H_2O, 0.1% formic acid, Buffer B = 80% acetonitrile, 0.1% formic acid, 19.9% H_2O, flow rate 400 nL/min). Eluted peptides were sprayed into a Q-Exactive HF-X MS (www.thermo.com) for data-independent acquisition. Survey scans were taken in the Orbi trap (45000 resolution, determined at m/z 200, mass range: 400–1,000 m/z). Fixed windows of 20 m/z (34 total) with 1 m/z overlapping margins were sequentially scanned and fragmented by HCD acquired in the Orbitrap at 15,000 resolutions.

Data-independent acquisition data analysis

Acquired spectra were processed using DIA-NN (v1.8.1, (Demichev et al. 2020), using the Robust LC (high precision) quantitation strategy with RT-dependent cross-referencing and Deep Learning enabled in library-free mode against Arabidopsis protein sequences available from Uniprot (www.uniprot.org), and search parameters were optimized by DIA-NN and results filtered at a precursor *FDR* of 1%.

Nanopore direct RNA-sequencing

Poly(A)-tailed RNA of 2 replicates per sample was extracted from Arabidopsis wild-type and *dus2* seedlings using 2 to 3 μg of total cellular RNA or in vitro–transcribed transcriptome RNA. Nanopore direct RNA-seq libraries were generated and barcoded following the manufacturer's instructions (SQK-RNA004). Barcodes were associated with read IDs using SeqTagger (Pryszcz et al. 2025). Raw files were basecalled using Dorado (v1.0.0: https://github.com/nanoporetech/dorado) with the following arguments: -v sup, inosine_m6A_2OmeA, 2OmeG,m5C_2OmeC, pseU_2OmeU, -emit-moves, and -min-qscore 10. BAM files were then demultiplexed by filtering for the relevant read IDs from SeqTagger using Samtools and fastq file conversion (Li et al. 2009; Pryszcz et al. 2025). Fastq files were mapped to the *Arabidopsis* transcriptome using Minimap2 (v2.29, parameter: -y, -ax map-ont, and -L) (Li, 2018). Nanocompore algorithm was utilized to detect *dus2* dependent modified sites (Leger et al. 2021). First, signal alignment was performed using Uncalled4 (v4.1.0) (Kovaka et al. 2021) with signal aligned BAM files used as input to Nanocompore (depleted condition: *dus2*, min coverage: 10, chi-squared q-value < 0.05, GMM log odds ratio > |0.3|).

Construction of co-expression networks

The co-expression networks were constructed using the WGCNA package with variance stabilizing transformed (VST)-normalized read counts with 34,130 transcripts across 96 samples (Langfelder and Horvath 2008). Initially, a soft threshold (Beta score) was applied to fit the scale-free topology model assumption which generates a minimum number to make the index curve flatten out reaching a high value (>0.85) (Yu et al. 2024b). Further, the adjacency matrix represented by gene expression was transformed into a topological overlap matrix (TOM) to classify genes using a dynamic tree-cut approach. Finally, genes that shared high-confidence correlation (abs[coefficient] > 0.8) were merged into the same module (parameter: deepsplit = 4, tree cut height = 0.2). The pairwise Pearson correlation between each gene from modules and the module-wise eigengene values was tested to characterize each gene's module membership (MM) under the same module. Lastly, the metabolite profiles, oxidative stress-related enzyme activities, and LI-6800-derived traits were integrated into the network using Pearson correlation between gene expression and these molecular phenotypes. Trait-correlated modules were selected based on their correlation level between MM scores and phenotypes (cutoff: $r > 0.5$, or $r < -0.5$, P value < 0.05). The correlation between gene expression and phenotypes was estimated as gene significance (GS) to interpret the importance of genes related to each molecular phenotype.

Functional and regulatory network analyses

Functional enrichment analysis of pathways (Kyoto Encyclopedia of Genes and Genomes [KEGG] database) and Gene Ontology (GO) analysis was performed to infer the biological function of genes associated with certain RCMs, transcripts assigned in co-expression modules, and differentially abundant transcripts. ShinyGO was used for GO and

KEGG enrichment for both sorghum and Arabidopsis (*FDR* < 0.05, (Ge et al. 2020). The protein-protein interactions (PPI) among genes present in the co-expression network were acquired from the STRING database (parameter: confidence level: > 0.7, (von Mering et al. 2003).

Data visualization and usage of databases

All statistical visualizations were generated in R (v4.3.2) with multiple packages. Briefly, plots include the line, boxplot, PCA, and enrichment graphs generated by the ggplot2 package, and heatmaps using the pheatmap package (R Core Team 2013). R Scripts used for plots were deposited in (https://rpubs.com/LeonYu/Main-Figures and https://rpubs.com/LeonYu/Supp-Figures). The integrated gene networks PPIs and co-expression derived from WGCNA were generated using Cytoscape (Shannon et al. 2003).

Accession numbers

SbDus1 (Sobic.010G262000), SbDus2 (Sobic.006G158100), SbDus3 (Sobic.006G038500), AtDus1 (AT5G67220), AtDus2 (AT3G49640), AtDus3 (AT3G63510), CHUP1 (AT3G25690), FBA6 (AT2G36460), SDH5 (AT1G47420), ENODL2 (AT4G27520), TRFX1 (AT3G02730), CP12-2 (AT3G62410), CHLG (AT3G51820), RPP0B (AT3G09200), AMY3 (AT1G69830), FUG1 (AT1G17220), FLU (AT3G14110), ATCAP1 (AT4G34490), emb2726 (AT4G29060), RPL5 (AT4G01310), HEME1 (AT3G14930), FBA8 (AT3G52930), ALDH2C4 (AT3G24503), GSA2 (AT3G48730), RPL10AB (AT2G27530), CRD1 (AT2G33420), PSAN (AT5G64040), LHCB2.1 (AT2G05100), LHCA1 (AT3G54890).

Supplementary material

Supplementary material is available at The Plant Cell online.

Acknowledgments

We would like to thank the members of the epitranscriptomic working group within the Nelson, Pauli, Schroeder, and Gregory labs for their insightful comments. We would like to thank Dr. Cliff Weil for insightful comments about the SAP, Dr. Tony Schilmiller and the MSU Mass Spectrometry and Metabolomics Core for assistance in metabolomics measurements and analysis. Many thanks to Dr. Alyssa Kearly for her assistance in technical proofing of the manuscript.

Author contributions

L.Y., G.M., A.E.A., E.H.L., B.D.G., A.D.L.N., and D.P. developed the experiment. G.M., S.C., B.R., and D.P. designed the field experiment and collected field-related data. A.C.N.D. and E.K.B. extracted RNA and performed other sorghum-related molecular experiments. A.E. provided accessions from the SAP for this study. L.Y., A.C.N.D. Ap.S., X.Z., and E.K.B. worked with the Arabidopsis *dus2* mutants. D.R.G. generated and contributed to the analysis of GMUCT data. G.M. and T.O. generated the metabolomics data. H.A. and G.B. generated the biochemical data related to oxidative stress status. R.H. and D.S. helped and provided expertise in acquiring physiological measurements for the Arabidopsis DUS2 mutants. L.Y. and S.J.S. worked on mRNA purification and hydrolysis. H.F. and Al.S. performed LC-MS/MS on dihydrouridine quantification. L.Y. analyzed all RNA-seq and developed co-expression networks, and omics data integration. L.Y., K.P., and S.J.S. analyzed epitranscriptomic data. L.Y., B.D.G., A.D.L.N., and D.P. wrote the manuscript.

Funding

This work was supported by the US National Science Foundation (NSF) Division of Integrative Organismal Systems (IOS) Plant Genome Research Program (PGRP) 2023310 (to A.D.L.N., E.H.L., D.P., and B.D.G.), NSF IOS PGRP 1849708 (to B.D.G.), NSF Division of Molecular and Cellular Biosciences (MCB) 2427729 (to B.D.G.), NSF PGRP 2102120 (to D.P. and A.D.L.N.), Department of Energy (DOE) DE-AR0001101 (to D.P.), DE-SC0023305 (to A.E. and D.P.), DE-SC0020401 (to A.E. and D.P.), Cotton Incorporated 18-384, 20-720, and 21-830 (to D.P.), NSF Division of Biological Infrastructure (DBI) 2019674 (to D.P. and A.D.L.N.), the Triad Foundation (to A.D.L.N.), a United States Department of Agriculture (USDA) Postdoctoral Fellowship #2024-67012-43106 (to H.F.), and the US National Institutes of Health (NIH) R35GM153298 (to A.I.S.).

Data availability

Transcriptome sequencing reads have been deposited in the National Center for Biotechnology Information (NCBI) BioProject database under the accession number: PRJNA1119650. Chromatograms of 5,6-dihydrouridine mass spectrometry data was deposited under massIVE online repository (ftp://massive.ucsd.edu/v09/MSV000097205/). Computational pipelines used for data analysis were deposited under the GitHub page (https://github.com/Leon-Yu0320/Sorghum_Range28). The R markdown files (R code) for data visualization in main figures and supplementary figures were deposited in Rpubs workspace (https://rpubs.com/LeonYu/Main-Figures and https://rpubs.com/LeonYu/Supp-Figures). All statistical analyses including parameters, degree of freedom, and test statistics were summarized in Table S17.

Conflicts of interest

The authors declare no competing interests.

References

Abreha KB et al. 2021. Sorghum in dryland: morphological, physiological, and molecular responses of sorghum under drought stress. Planta. 255:20. https://doi.org/10.1007/s00425-021-03799-7.

Aebi H. 1984. [13] catalase in vitro. Methods Enzymol. 105:121–126. https://doi.org/10.1016/S0076-6879(84)05016-3.

Alizadeh MR et al. 2020. A century of observations reveals increasing likelihood of continental-scale compound dry-hot extremes. Sci Adv. 6: eaaz4571. https://doi.org/10.1126/sciadv.aaz4571.

Anderson SJ et al. 2018. N^6-methyladenosine inhibits local ribonucleolytic cleavage to stabilize mRNAs in Arabidopsis. Cell Rep. 25:1146–1157.e3. https://doi.org/10.1016/j.celrep.2018.10.020.

Arribas-Hernández L et al. 2018. An m^6A-YTH module controls developmental timing and morphogenesis in Arabidopsis. Plant Cell. 30: 952–967. https://doi.org/10.1105/tpc.17.00833.

Benzie I, Strain J. 1999. Ferric reducing/antioxidant power assay: direct measure of total antioxidant activity of biological fluids and modified version for simultaneous measurement of total antioxidant power and ascorbic acid concentration. Methods Enzymol. 299:15–27. https://doi.org/10.1016/S0076-6879(99)99005-5.

Boatwright JL et al. 2022. Sorghum association panel whole-genome sequencing establishes cornerstone resource for dissecting genomic diversity. Plant J. 111:888–904. https://doi.org/10.1111/tpj.15853.

Bolger AM, Lohse M, Usadel B. 2014. Trimmomatic: a flexible trimmer for illumina sequence data. Bioinformatics. 30:2114–2120. https://doi.org/10.1093/bioinformatics/btu170.

Boyles RE, Brenton ZW, Kresovich S. 2019. Genetic and genomic resources of sorghum to connect genotype with phenotype in contrasting environments. Plant J. 97:19–39. https://doi.org/10.1111/tpj.14113.

Brazel AJ, Manoj NS, Turck F, Ó'Maoiléidigh DS. 2025. Measuring CO_2 assimilation of Arabidopsis thaliana whole plants and seedlings. Plant Sci. 350:112295. https://doi.org/10.1016/j.plantsci.2024.112295.

Brégeon D et al. 2022. Dihydrouridine in the transcriptome: new life for this ancient RNA chemical modification. ACS Chem Biol. 17:1638–1657. https://doi.org/10.1021/acschembio.2c00307.

Burgess SJ. 2023. QIAGEN RNeasy plant RNA extraction protocol (modified). protocols.io. Protocol Integer ID: 78347. https://doi.org/10.17504/protocols.io.cqrjvv4n.

Cai J, Shen L, Kang H, Xu T. 2025. RNA modifications in plant adaptation to abiotic stresses. Plant Commun. 6:101229. https://doi.org/10.1016/j.xplc.2024.101229.

Chen P, Jäger G, Zheng B. 2010. Transfer RNA modifications and genes for modifying enzymes in Arabidopsis thaliana. BMC Plant Biol. 10:201. https://doi.org/10.1186/1471-2229-10-201.

Chen Y, Chen L, Lun ATL, Baldoni PL, Smyth GK. 2025. Edger v4: powerful differential analysis of sequencing data with expanded functionality and improved support for small counts and larger datasets. Nucleic Acids Res. 53:gkaf018. https://doi.org/10.1093/nar/gkaf018.

Cheng C-Y et al. 2017. Araport11: a complete reannotation of the Arabidopsis thaliana reference genome. Plant J. 89:789–804. https://doi.org/10.1111/tpj.13415.

Cheng Q et al. 2021. Coordination of m^6A mRNA methylation and gene transcriptome in rice response to cadmium stress. Rice (N Y). 14:62. https://doi.org/10.1186/s12284-021-00502-y.

Cruciani S et al. 2025. De novo basecalling of RNA modifications at single molecule and nucleotide resolution. Genome Biol. 26:38. https://doi.org/10.1186/s13059-025-03498-6.

da Bernardino KC et al. 2024. Genetic loci associated with sorghum drought tolerance in multiple environments and their sensitivity to environmental covariables. Theor Appl Genet. 137:259. https://doi.org/10.1007/s00122-024-04761-3.

Dai W et al. 2021. Activity-based RNA-modifying enzyme probing reveals DUS3L-mediated dihydrouridylation. Nat Chem Biol. 17:1178–1187. https://doi.org/10.1038/s41589-021-00874-8.

Das K, Roychoudhury A. 2014. Reactive oxygen species (ROS) and response of antioxidants as ROS-scavengers during environmental stress in plants. Front Environ Sci. 2:53. https://doi.org/10.3389/fenvs.2014.00053.

Demichev V, Messner CB, Vernardis SI, Lilley KS, Ralser M. 2020. DIA-NN: neural networks and interference correction enable deep proteome coverage in high throughput. Nat Methods. 17:41–44. https://doi.org/10.1038/s41592-019-0638-x.

Dobin A, Gingeras TR. 2015. Mapping RNA-Seq reads with STAR. Curr Protoc Bioinformatics. 51:11.14.1–11.14.19. https://doi.org/10.1002/0471250953.bi1114s51.

Dominissini D et al. 2012. Topology of the human and mouse m6A RNA methylomes revealed by m6A-seq. Nature. 485:201–206. https://doi.org/10.1038/nature11112.

Draycott AS et al. 2022. Transcriptome-wide mapping reveals a diverse dihydrouridine landscape including mRNA. PLoS Biol. 20:e3001622. https://doi.org/10.1371/journal.pbio.3001622.

Edelheit S, Schwartz S, Mumbach MR, Wurtzel O, Sorek R. 2013. Transcriptome-wide mapping of 5-methylcytidine RNA modifications in bacteria, archaea, and yeast reveals m5C within archaeal mRNAs. PLoS Genet. 9:e1003602. https://doi.org/10.1371/journal.pgen.1003602.

Fahlgren N et al. 2015. A versatile phenotyping system and analytics platform reveals diverse temporal responses to water availability in Setaria. Mol Plant. 8:1520–1535. https://doi.org/10.1016/j.molp.2015.06.005.

Feierabend J, Beevers H. 1972. Developmental studies on microbodies in wheat leaves: I. Conditions influencing enzyme development: I. Conditions influencing enzyme development. Plant Physiol. 49:28–32. https://doi.org/10.1104/pp.49.1.28.

Finet O et al. 2022a. Transcription-wide mapping of dihydrouridine reveals that mRNA dihydrouridylation is required for meiotic chromosome segregation. Mol Cell. 82:404–419.e9. https://doi.org/10.1016/j.molcel.2021.11.003.

Finet O, Yague-Sanz C, Marchand F, Hermand D. 2022b. The dihydrouridine landscape from tRNA to mRNA: a perspective on synthesis, structural impact and function. RNA Biol. 19:735–750. https://doi.org/10.1080/15476286.2022.2078094.

Ganguly DR et al. 2025. mRNA ADENOSINE METHYLASE promotes drought tolerance through N^6-methyladenosine-dependent and independent impacts on mRNA regulation in Arabidopsis. New Phytol. 245:183–199. https://doi.org/10.1111/nph.20227.

Garalde DR et al. 2018. Highly parallel direct RNA sequencing on an array of nanopores. Nat Methods. 15:201–206. https://doi.org/10.1038/nmeth.4577.

Ge SX, Jung D, Yao R. 2020. ShinyGO: a graphical gene-set enrichment tool for animals and plants. Bioinformatics. 36:2628–2629. https://doi.org/10.1093/bioinformatics/btz931.

Gilliham M, Able JA, Roy SJ. 2017. Translating knowledge about abiotic stress tolerance to breeding programmes. Plant J. 90:898–917. https://doi.org/10.1111/tpj.13456.

Glaszmann JC, Kilian B, Upadhyaya HD, Varshney RK. 2010. Accessing genetic diversity for crop improvement. Curr Opin Plant Biol. 13:167–173. https://doi.org/10.1016/j.pbi.2010.01.004.

Gregory BD et al. 2008. A link between RNA metabolism and silencing affecting Arabidopsis development. Dev Cell. 14:854–866. https://doi.org/10.1016/j.devcel.2008.04.005.

Harcourt EM, Kietrys AM, Kool ET. 2017. Chemical and structural effects of base modifications in messenger RNA. Nature. 541:339–346. https://doi.org/10.1038/nature21351.

Helm M, Motorin Y. 2017. Detecting RNA modifications in the epitranscriptome: predict and validate. Nat Rev Genet. 18:275–291. https://doi.org/10.1038/nrg.2016.169.

Hodges DM, DeLong JM, Forney CF, Prange RK. 1999. Improving the thiobarbituric acid-reactive-substances assay for estimating lipid peroxidation in plant tissues containing anthocyanin and other interfering compounds. Planta. 207:604–611. https://doi.org/10.1007/s004250050524.

Jia T, Le BH. 2020. RNA stability measurements using RT-qPCR in *Arabidopsis* seedlings. Bio Protoc. 10:e3680. https://doi.org/10.21769/BioProtoc.3680.

Ju C-W et al. 2025. Quantitative CRACI reveals transcriptome-wide distribution of RNA dihydrouridine at base resolution. Nat Commun. 16:8863. https://doi.org/10.1038/s41467-025-63918-w.

Kato T et al. 2005. A novel human tRNA-dihydrouridine synthase involved in pulmonary carcinogenesis. Cancer Res. 65:5638–5646. https://doi.org/10.1158/0008-5472.CAN-05-0600.

Khoury CK et al. 2022. Crop genetic erosion: understanding and responding to loss of crop diversity. New Phytol. 233:84–118. https://doi.org/10.1111/nph.17733.

Kim D et al. 2013. TopHat2: accurate alignment of transcriptomes in the presence of insertions, deletions and gene fusions. Genome Biol. 14: R36. https://doi.org/10.1186/gb-2013-14-4-r36.

Kim D, Paggi JM, Park C, Bennett C, Salzberg S. 2019. Graph-based genome alignment and genotyping with HISAT2 and HISAT-genotype. Nat Biotechnol. 37:907–915. https://doi.org/10.1038/s41587-019-0201-4.

Kovaka S, Fan Y, Ni B, Timp W, Schatz MC. 2021. Targeted nanopore sequencing by real-time mapping of raw electrical signal with UNCALLED. Nat Biotechnol. 39:431–441. https://doi.org/10.1038/s41587-020-0731-9.

Krueger F. 2015. Trim galore!: a wrapper around cutadapt and FastQC to consistently apply adapter and quality trimming to FastQ files, with extra functionality for RRBS data. Babraham Institute.

Langfelder P, Horvath S. 2008. WGCNA: an R package for weighted correlation network analysis. BMC Bioinformatics. 9:559. https://doi.org/10.1186/1471-2105-9-559.

LaPierre N, Egan R, Wang W, Wang Z. 2019. De novo nanopore read quality improvement using deep learning. BMC Bioinformatics. 20:552. https://doi.org/10.1186/s12859-019-3103-z.

Lee W-C et al. 2020. Widespread exon junction complex footprints in the RNA degradome mark mRNA degradation before steady state translation. Plant Cell. 32:904–922. https://doi.org/10.1105/tpc.19.00666.

Leger A et al. 2021. RNA modifications detection by comparative nanopore direct RNA sequencing. Nat Commun. 12:7198. https://doi.org/10.1038/s41467-021-27393-3.

Levine R, Williams JA, Stadtman EP, Shacter E. 1994. Carbonyl assays for determination of oxidatively modified proteins. Methods Enzymol. 233:346–357. https://doi.org/10.1016/S0076-6879(94)33040-9.

Li H. Aligning sequence reads, clone sequences and assembly contigs with BWA-MEM. arXiv 3997v2. https://doi.org/10.48550/arXiv.1303.3997, 16 March 2013, preprint: not peer reviewed.

Li H et al. 2009. The sequence alignment/map format and SAMtools. Bioinformatics. 25:2078–2079. https://doi.org/10.1093/bioinformatics/btp352.

Li H. 2018. Minimap2: pairwise alignment for nucleotide sequences. Bioinformatics. 34:3094–3100. https://doi.org/10.1093/bioinformatics/bty191.

Li H et al. 2025. Quantitative RNA pseudouridine maps reveal multilayered translation control through plant rRNA, tRNA and mRNA pseudouridylation. Nat Plants. 11:234–247. https://doi.org/10.1038/s41477-024-01894-7.

Li L et al. 2022. Enzymes degraded under high light maintain proteostasis by transcriptional regulation in *Arabidopsis*. Proc Natl Acad Sci U S A. 119:e2121362119. https://doi.org/10.1073/pnas.2121362119.

Li X et al. 2016. Transcriptome-wide mapping reveals reversible and dynamic N(1)-methyladenosine methylome. Nat Chem Biol. 12:311–316. https://doi.org/10.1038/nchembio.2040.

Liao Y, Smyth G, Shi W. 2014. featureCounts: an efficient general purpose program for assigning sequence reads to genomic features. Bioinformatics. 30:923–930. https://doi.org/10.1093/bioinformatics/btt656.

Liu H et al. 2019. Accurate detection of m^{6}A RNA modifications in native RNA sequences. Nat Commun. 10:4079. https://doi.org/10.1038/s41467-019-11713-9.

Liu H et al. 2020. A natural variation in *PLEIOTROPIC DEVELOPMENTAL DEFECTS* uncovers a crucial role for chloroplast tRNA modification in translation and plant development. Plant Cell. 32:2345–2366. https://doi.org/10.1105/tpc.19.00660.

Liu K et al. 2025. N^6-methyladenosine modifications stabilize phosphate starvation response-related mRNAs in plant adaptation to nutrient-deficient stress. Nat Commun. 16:4093. https://doi.org/10.1038/s41467-025-59331-y.

Lobell DB et al. 2008. Prioritizing climate change adaptation needs for food security in 2030. Science. 319:607–610. https://doi.org/10.1126/science.1152339.

Lombard M et al. 2022. Evolutionary diversity of Dus2 enzymes reveals novel structural and functional features among members of the RNA dihydrouridine synthases family. Biomolecules. 12:1760. https://doi.org/10.3390/biom12121760.

Love MI, Huber W, Anders S. 2014. Moderated estimation of fold change and dispersion for RNA-Seq data with DESeq2. Genome Biol. 15:550. https://doi.org/10.1186/s13059-014-0550-8.

Luo J-H et al. 2020. Natural variation in RNA m^{6}A methylation and its relationship with translational status. Plant Physiol. 182:332–344. https://doi.org/10.1104/pp.19.00987.

McCormick RF et al. 2018. The Sorghum bicolor reference genome: improved assembly, gene annotations, a transcriptome atlas, and signatures of genome organization. Plant J. 93:338–354. https://doi.org/10.1111/tpj.13781.

McKenna A et al. 2010. The genome analysis toolkit: a MapReduce framework for analyzing next-generation DNA sequencing data. Genome Res. 20:1297–1303. https://doi.org/10.1101/gr.107524.110.

McLaren W et al. 2016. The ensembl variant effect predictor. Genome Biol. 17:122. https://doi.org/10.1186/s13059-016-0974-4.

Melandri G et al. 2020. Biomarkers for grain yield stability in rice under drought stress. J Exp Bot. 71:669–683. https://doi.org/10.1093/jxb/erz221.

Merret R et al. 2013. XRN4 and LARP1 are required for a heat-triggered mRNA decay pathway involved in plant acclimation and survival during thermal stress. Cell Rep. 5:1279–1293. https://doi.org/10.1016/j.celrep.2013.11.019.

Meyer KD et al. 2012. Comprehensive analysis of mRNA methylation reveals enrichment in 3′ UTRs and near stop codons. Cell. 149: 1635–1646. https://doi.org/10.1016/j.cell.2012.05.003.

Morris GP et al. 2013. Population genomic and genome-wide association studies of agroclimatic traits in sorghum. Proc Natl Acad Sci U S A. 110:453–458. https://doi.org/10.1073/pnas.1215985110.

Murashige T, Skoog F. 1962. A revised medium for rapid growth and bio assays with tobacco tissue cultures. Physiol Plant. 15:473–497. https://doi.org/10.1111/j.1399-3054.1962.tb08052.x.

Murshed R, Lopez-Lauri F, Sallanon H. 2008. Microplate quantification of enzymes of the plant ascorbate-glutathione cycle. Anal Biochem. 383: 320–322. https://doi.org/10.1016/j.ab.2008.07.020.

Nguyen L-T, Schmidt HA, von Haeseler A, Minh BQ. 2015. IQ-TREE: a fast and effective stochastic algorithm for estimating maximum-likelihood phylogenies. Mol Biol Evol. 32:268–274. https://doi.org/10.1093/molbev/msu300.

Notarnicola RF et al. Molecular signatures of heat tolerance and sensitivity in the alpine plant Wahlenbergia ceracea during moderate warming. bioRxiv 559694. https://doi.org/10.1101/2023.09.27.559694, 4 January 2025, preprint: not peer reviewed.

Obata T et al. 2015. Metabolite profiles of maize leaves in drought, heat, and combined stress field trials reveal the relationship between metabolism and grain yield. Plant Physiol. 169:2665–2683. https://doi.org/10.1104/pp.15.01164.

Palos K, Nelson Dittrich AC, Lyons EH, Gregory BD, Nelson ADL. 2024. Comparative analyses suggest a link between mRNA splicing, stability, and RNA covalent modifications in flowering plants. BMC Plant Biol. 24: 768. https://doi.org/10.1186/s12870-024-05486-7.

Pardo J et al. 2023. Cross-species predictive modeling reveals conserved drought responses between maize and sorghum. Proc Natl Acad Sci U S A. 120:e2216894120. https://doi.org/10.1073/pnas.2216894120.

Pardo J, VanBuren R. 2021. Evolutionary innovations driving abiotic stress tolerance in C4 grasses and cereals. Plant Cell. 33:3391–3401. https://doi.org/10.1093/plcell/koab205.

Park S-H et al. 2012. Posttranscriptional control of photosynthetic mRNA decay under stress conditions requires 3′ and 5′ untranslated regions and correlates with differential polysome association in rice. Plant Physiol. 159:1111–1124. https://doi.org/10.1104/pp.112.194928.

Porra RJ, Thompson WA, Kriedemann PE. 1989. Determination of accurate extinction coefficients and simultaneous equations for assaying chlorophylls a and b extracted with four different solvents: verification of the concentration of chlorophyll standards by atomic absorption spectroscopy. Biochim Biophys Acta Bioenerg. 975:384–394. https://doi.org/10.1016/s0005-2728(89)80347-0.

Prall W et al. 2023. Pathogen-induced m6A dynamics affect plant immunity. Plant Cell. 35:4155–4172. https://doi.org/10.1093/plcell/koad224.

Pryszcz LP et al. 2025. Rapid and accurate demultiplexing of direct RNA nanopore sequencing data with SeqTagger. Genome Res. 35:956–966. https://doi.org/10.1101/gr.279290.124.

Purcell S et al. 2007. PLINK: a tool set for whole-genome association and population-based linkage analyses. Am J Hum Genet. 81:559–575. https://doi.org/10.1086/519795.

R Core Team. 2013. R: a language and environment for statistical computing. Foundation for Statistical Computing.

Rider LW, Ottosen MB, Gattis SG, Palfey BA. 2009. Mechanism of dihydrouridine synthase 2 from yeast and the importance of modifications for efficient tRNA reduction. J Biol Chem. 284:10324–10333. https://doi.org/10.1074/jbc.M806137200.

Riewe D et al. 2012. A tyrosine aminotransferase involved in tocopherol synthesis in Arabidopsis: tyrosine aminotransferase affecting tocopherols. Plant J. 71:850–859. https://doi.org/10.1111/j.1365-313X.2012.05035.x.

Roundtree IA, Evans ME, Pan T, He C. 2017. Dynamic RNA modifications in gene expression regulation. Cell. 169:1187–1200. https://doi.org/10.1016/j.cell.2017.05.045.

Ryvkin P et al. 2013. HAMR: high-throughput annotation of modified ribonucleotides. RNA. 19:1684–1692. https://doi.org/10.1261/rna.036806.112.

Schwitzguebel JP, Siegenthaler PA. 1984. Purification of peroxisomes and mitochondria from spinach leaf by percoll gradient centrifugation. Plant Physiol. 75:670–674. https://doi.org/10.1104/pp.75.3.670.

Shannon P et al. 2003. Cytoscape: a software environment for integrated models of biomolecular interaction networks. Genome Res. 13:2498–2504. https://doi.org/10.1101/gr.1239303.

Shao Y, Ma J, Zhang S, Xu Y, Yu H. 2025. NERD-dependent m^6A modification of the nascent FLC transcript regulates flowering time in Arabidopsis. Nat Plants. 11:468–482. https://doi.org/10.1038/s41477-025-01945-7.

Sharma B, Prall W, Bhatia G, Gregory BD. 2023. The diversity and functions of plant RNA modifications: what we know and where we go from here. Annu Rev Plant Biol. 74:53–85. https://doi.org/10.1146/annurev-arplant-071122-085813.

Singh A, Newton L, Schnable JC, Thompson AM. 2025. Unveiling shared genetic regulators of plant architectural and biomass yield traits in the Sorghum association panel. J Exp Bot. 76:1625–1643. https://doi.org/10.1093/jxb/eraf012.

Sipa K et al. 2007. Effect of base modifications on structure, thermodynamic stability, and gene silencing activity of short interfering RNA. RNA. 13:1301–1316. https://doi.org/10.1261/rna.538907.

Sorenson RS, Deshotel MJ, Johnson K, Adler FR, Sieburth LE. 2018. *Arabidopsis* mRNA decay landscape arises from specialized RNA decay substrates, decapping-mediated feedback, and redundancy. Proc Natl Acad Sci U S A. 115:E1485–E1494. https://doi.org/10.1073/pnas.1712312115.

Tan K-T, Ding L-W, Wu C-S, Tenen DG, Yang H. 2021. Repurposing RNA sequencing for discovery of RNA modifications in clinical cohorts. Sci Adv. 7:eabd2605. https://doi.org/10.1126/sciadv.abd2605.

Tang Y et al. 2020. OsNSUN2-mediated 5-methylcytosine mRNA modification enhances rice adaptation to high temperature. Dev Cell. 53:272–286.e7. https://doi.org/10.1016/j.devcel.2020.03.009.

Tarasov A, Vilella AJ, Cuppen E, Nijman IJ, Prins P. 2015. Sambamba: fast processing of NGS alignment formats. Bioinformatics. 31:2032–2034. https://doi.org/10.1093/bioinformatics/btv098.

Toubdji S et al. 2024. Exploring a unique class of flavoenzymes: identification and biochemical characterization of ribosomal RNA dihydrouridine synthase. Proc Natl Acad Sci U S A. 121:e2401981121. https://doi.org/10.1073/pnas.2401981121.

Vandivier LE et al. 2015. Chemical modifications mark alternatively spliced and uncapped messenger RNAs in Arabidopsis. Plant Cell. 27:3024–3037. https://doi.org/10.1105/tpc.15.00591.

Varoquaux N et al. 2019. Transcriptomic analysis of field-droughted sorghum from seedling to maturity reveals biotic and metabolic responses. Proc Natl Acad Sci U S A. 116:27124–27132. https://doi.org/10.1073/pnas.1907500116.

von Mering C et al. 2003. STRING: a database of predicted functional associations between proteins. Nucleic Acids Res. 31:258–261. https://doi.org/10.1093/nar/gkg034.

Wase N, Abshire N, Obata T. 2022. High-throughput profiling of metabolic phenotypes using high-resolution GC-MS. Methods Mol Biol. 2539:235–260. https://doi.org/10.1007/978-1-0716-2537-8_19.

Willmann MR, Berkowitz ND, Gregory BD. 2014. Improved genome-wide mapping of uncapped and cleaved transcripts in eukaryotes–GMUCT 2.0. Methods. 67:64–73. https://doi.org/10.1016/j.ymeth.2013.07.003.

Wu X et al. 2022. Genomic footprints of sorghum domestication and breeding selection for multiple end uses. Mol Plant. 15:537–551. https://doi.org/10.1016/j.molp.2022.01.002.

Wu Y et al. 2024. Transfer learning enables identification of multiple types of RNA modifications using nanopore direct RNA sequencing. Nat Commun. 15:4049. https://doi.org/10.1038/s41467-024-48437-4.

Yang W et al. 2020. The N^1-methyladenosine methylome of petunia mRNA. Plant Physiol. 183:1710–1724. https://doi.org/10.1104/pp.20.00382.

Yu F et al. 2011. Molecular basis of dihydrouridine formation on tRNA. Proc Natl Acad Sci U S A. 108:19593–19598. https://doi.org/10.1073/pnas.1112352108.

Yu L et al. 2024a. Regulation of a single inositol 1-phosphate synthase homeologue by HSFA6B contributes to fibre yield maintenance under drought conditions in upland cotton. Plant Biotechnol J. 22:2756–2772. https://doi.org/10.1111/pbi.14402.

Yu L et al. 2024b. Development of a mobile, high-throughput, and low-cost image-based plant growth phenotyping system. Plant Physiol. 196:810–829. https://doi.org/10.1093/plphys/kiae237.

Yu X, Sharma B, Gregory BD. 2021. The impact of epitranscriptomic marks on post-transcriptional regulation in plants. Brief Funct Genomics. 20:113–124. https://doi.org/10.1093/bfgp/elaa021.

Zhang Q et al. 2006a. A simple 96-well microplate method for estimation of total polyphenol content in seaweeds. J Appl Phycol. 18:445–450. https://doi.org/10.1007/s10811-006-9048-4.

Zhang X, Henriques R, Lin S-S, Niu Q-W, Chua N-H. 2006b. Agrobacterium-mediated transformation of Arabidopsis thaliana using the floral dip method. Nat Protoc. 1:641–646. https://doi.org/10.1038/nprot.2006.97.

Zhou L et al. 2022. M^6 A-mediated regulation of crop development and stress responses. Plant Biotechnol J. 20:1447–1455. https://doi.org/10.1111/pbi.13792.